

UNCLASSIFIED

AD NUMBER
AD851749
NEW LIMITATION CHANGE
TO Approved for public release, distribution unlimited
FROM Distribution: Further dissemination only as directed by Advanced Research Projects Agency, Washington, DC 20301, 06 MAR 1969, or higher DoD authority.
AUTHORITY
USNOL ltr, 12 Dec 1972

THIS PAGE IS UNCLASSIFIED

NO

NOTHING MORE

MODEL STUDIES OF THE BEHAVIOR OF UNDERWATER EXPLOSION BUBBLES
IN CONTACT WITH A RIGID BOTTOM

By

John F. Goertner

John R. Hendrickson

Richard G. Leamon

AD 851749

ABSTRACT: The behavior of the explosion bubble in contact with a rigid bottom was investigated on a small scale using high speed photography. The experiments were carried out in a vacuum tank with 0.2-gram charges fired above a 2-inch thick aluminum plate. Test conditions were varied by small increments so that a complete sequence of changing bubble behavior--from bubbles which remained intact on the bottom, to bubbles which split into two or more parts, to bubbles which separated from the bottom intact--was observed. A qualitative description of the bubble behavior along with its dimensions at maximum volume and--for strongly migrating bubbles--at minimum volume is presented in dimensionless form as a function of the inverse Froude number, the amplitude of oscillation, and the distance to the water surface. The qualitative behavior appears to be different from that observed with HE field tests on cratering bottoms. Other factors being equal, there appears to be a greater tendency for a bubble to stick to a cratering bottom.

UNDERWATER EXPLOSIONS DIVISION
EXPLOSIONS RESEARCH DEPARTMENT
U. S. NAVAL ORDNANCE LABORATORY
WHITE OAK, SILVER SPRING, MARYLAND

**Best
Available
Copy**

NOLTR 68-207

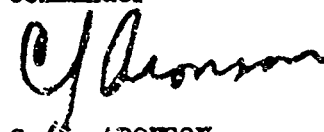
6 March 1969

MODEL STUDIES OF THE BEHAVIOR OF UNDERWATER EXPLOSION BUBBLES IN CONTACT WITH
A RIGID BOTTOM

The work described here was sponsored by the Advanced Research Projects Agency of the Department of Defense. The investigation of bottom phenomena for this sponsor was initiated under Task NOL-785/ARPA, titled "Source Level and Containment Mechanism Studies of Underwater Explosions," and was continued under Task NOL-150/NRDL, titled "Underwater Explosion On-Site Inspection Research." The results reported represent a first attempt to analyze a series of bottom shots in a laboratory tank facility, and the conclusions are considered to be preliminary. The data have applications in the study of the damaging effects of conventional weapons and in the investigation of the possibility of the containment of the products of a clandestine nuclear test at sea by firing on the bottom. Mention of commercially available products in this report does not constitute criticism or endorsement by the Laboratory.

The new experiments reported here were carried out by P. S. Sherman and R. G. Leamon. The authors wish to acknowledge the considerable editorial assistance rendered by Dr. E. Swift, Jr. and Dr. G. A. Young.

E. F. SCHREITER
Captain, USN
Commander


C. S. ARONSON
By direction

CONTENTS

	Page
1. INTRODUCTION	1
1.1 Background	1
2. MODEL TEST RESULTS	2
2.1 Method of Modeling	2
2.2 Bubble Migration Behavior	3
2.3 Experimental Results	4
3. COMPARISON WITH PROTOTYPE DATA	7
3.1 Equations for Comparing Model and Prototype Data	7
3.2 Comparison with Prototype Data for Cratering Bottoms	9
3.3 Observations of Enhanced Migration and Jetting	11
4. SUMMARY OF RESULTS	12
5. CONCLUSIONS AND RECOMMENDATIONS	12
REFERENCES	14
APPENDIX A - CALCULATION OF MODEL PARAMETERS	A-1
APPENDIX B - ANALYSIS OF UNCERTAINTIES IN THE MODEL TESTS	B-1
APPENDIX C - HIGH-GRAVITY TANK TESTS ON A NON-CRATERING BOTTOM	C-1
APPENDIX D - EXPERIMENTAL DETAILS	D-1

ILLUSTRATIONS

Figure	Title	
1	Sticking Bubble	17
2	Splitting Bubble	18
3	Splitting Bubble	19
4	Weakly Migrating Bubble (Intermediate Case)	20
5	Strongly Migrating Bubble	21
6	Behavior of Bubbles on Non-Cratering Bottom as a Function of $(gt^2/A_{max})_c$ and $(A_{min}/A_{max})_c$	23
7	Reduced Equivalent Radius $(A_{max})_{eq}/(A_{max})_c$ at First Maximum-- Non-Cratering Bottom	24
8	Reduced Diameter $D_{max}/(A_{max})_c$ at First Maximum--Non-Cratering Bottom.	25
9	Reduced Height $H_{max}/(A_{max})_c$ at First Maximum--Non-Cratering Bottom.	26
10	Height-to-Diameter Ratio H_{max}/D_{max} at First Maximum--Non-Cratering Bottom	27

Figure	Title	Page
11	Observations of Jet Impact for Migrating Bubbles as a Function of $(gT^2/A_{\max})_c$ and $(A_{\max}/d)_c$ -- Non-Cratering Bottom.	28
12	Different Migrating Bubble Behavior--At a Time Just Before the First Minimum	29
13	Comparison of Reduced First Period Bubble Migration With and Without Bottom--Strongly Migrating Case, $d = 1$ ft	30
14	Comparison of Reduced First Period Bubble Migration With and Without Bottom--Strongly Migrating Case, $d = 2$ ft	31
15	Reduced Minimum Diameter, $D_{\min}/(A_{\max})_c$ as a Function of $(gT^2/A_{\max})_c$ and $(A_{\min}/(A_{\max})_c)$ -- Strongly Migrating Case, Non-Cratering Bottom.	33
16	Comparison of Non-Cratering Model Behavior with Observations from Full-Scale Tests.	34
17	Comparison of Non-Cratering Model Behavior with Estimates from Field Tests	35
A-1	Ratio J^* as a Function of P_{vap}/Z for 0.2-gm Lead Azide Charges in NOL Vacuum Tank	A-6
A-2	Ratio K^* as a Function of P_{vap}/Z for 0.2-gm Lead Azide Charges in NOL Vacuum Tank	A-7
C-1	Behavior of High-Gravity Tank Bubbles on a Non-Cratering Bottom as a Function of $(gT^2/A_{\max})_c$ and $(A_{\min}/A_{\max})_c$	C-2

TABLES

Table	Title	Page
1	Experimental Data from Shots on Rigid Bottom	36
2	Characteristic Numbers and Dimensionless Data for Shots on Rigid Bottom	38
3	Measured Data at First Bubble Minimum for Strongly Migrating Bubbles.	40
4	Some Prototype Bubble Parameters	8
A-1	Experimental Data from Control Shots--1967 Test Program.	A-8
A-2	Computed Data from Control Shots--1967 Test Program.	A-9
B-1	Comparison of Vacuum Tank and Field Test Uncertainties	B-3

LIST OF SYMBOLS

A_{\max}	= Maximum bubble radius (ft)
$(A_{\max})_{eq}$	= Radius of hemisphere of volume equal to maximum volume of bottom shot bubble (ft)
$(A_{\max})_c$	= Maximum bubble radius of control shot (ft)
A_{\min}	= Minimum bubble radius for a non-migrating bubble (ft)
c	= Subscript indicating control shot
d	= Charge depth (ft)
D_{\max}	= Diameter of bottom shot bubble at maximum volume (ft)
D_{\min}	= Diameter of strongly migrating bottom shot bubble at instant of jet impact (ft)
g	= Acceleration of gravity (ft/sec ²)
H_{\max}	= Height of bottom shot bubble at maximum bubble volume (ft)
J	= Bubble radius coefficient in test tank (ft ^{4/3} /lb ^{1/3})
J_{∞}	= Bubble radius coefficient in infinite water (ft ^{4/3} /lb ^{1/3})
K	= Bubble period coefficient in test tank (sec-ft ^{5/6} /lb ^{1/3})
K_{∞}	= Bubble period coefficient in infinite water (sec-ft ^{5/6} /lb ^{1/3})
N	= Bubble minimum radius coefficient (ft ^{-1/3})
P_{air}	= Air pressure (ft of water)
P_{\max}	= (Bubble parameter defined on page A-5)
$(P_{\max})_0$	= Minimum pressure inside bubble when no boiling occurs (ft of fresh water)
P_{vap}	= Vapor pressure of water (ft of fresh water)
R	= Radius of cylindrical test tank (ft)
Ratio J^0	= Change in bubble maximum radius due to presence of test tank

NUMBER 68-207

Ratio K^O = Change in bubble period due to presence of test tank

Ratio J^* = Change in bubble maximum radius due to boiling

Ratio K^* = Change in bubble period due to boiling

s = Standard deviation estimate

T = First bubble period (sec)

T_c = First bubble period of control shot (sec)

W = Charge weight (lbs)

Z = Hydrostatic pressure at depth of explosion (ft of water)

α = Free-surface correction coefficient for bubble period

γ = Adiabatic exponent for gas inside bubble

δ = Upward displacement measured from rigid bottom (from point of explosion on control shot) (ft)

δ_{center} = Upward displacement at time T , measured to center of bubble (ft)

δ_{top} = Upward displacement at time T , measured to top of bubble (ft)

MODEL STUDIES OF THE BEHAVIOR OF UNDERWATER EXPLOSION BUBBLE
IN CONTACT WITH A RIGID BOTTOM

1. INTRODUCTION

1.1 Background

When a conventional high explosive, such as TNT, is detonated under water, a shock wave is emitted and a bubble of gaseous explosion products is formed. In general, this bubble oscillates and migrates toward the surface, its behavior depending on the charge weight, depth, and the proximity of nearby surfaces. As early as World War II, it was known that the migration of a bubble formed by an explosion in the vicinity of the sea bed would differ from the migration of a bubble produced by the same explosive charge at the same depth in free water*. Since a migrating bubble is capable of damaging ships and submarines, bottom proximity could affect the damaging capabilities of mines, and detailed studies of the phenomena were conducted (e.g., Shiffman and Friedman, 1944)**.

In general, it was believed that the sea bottom would reduce the upward migration; however, the process was not fully understood and the theoretical treatments were not entirely successful (Cole, 1948). In 1953, Snay re-examined the effects of the sea bottom on bubble migration and presented new damage curves for mines. He made some use of small scale information acquired in the Naval Ordnance Laboratory Vacuum Tank (static tank) in 1952, but relied mostly on full-scale data for his damage predictions.

In 1961, Murray, Santamaria, and Clifford utilized the data published by Snay (1953) and field test data from other sources to develop a means of estimating the effect of the bottom on bubble migration. Even at this stage, a considerable amount of speculation, based on indirect information, was needed in order to obtain engineering-type estimates.

In 1965, the Naval Ordnance Laboratory began a study of the possibility of concealment of the evidence of a clandestine nuclear test in the ocean. As the presence of a bottom would, in some cases, result in suppression of the upward bubble migration, it was believed that it might be possible to conduct such a test

* The term "free-water explosion" refers to an explosion remote from the bottom.

** References are listed on page 14.

at a selected depth on the bottom and have no fission products arrive at the surface, even though a free-water nuclear test at the same charge depth would result in the formation of a radioactive surface pool. As the available data were not adequate to establish the critical bottom depth for the elimination of bubble migration, a new series of tests was conducted in the NOL High-Gravity Tank*. These data showed discrepancies with the previous Vacuum Tank study (Sherman, 1965) and with the available field test data (Snay, 1953; Murray, et al, 1961; Young, 1968).

In an attempt to resolve these discrepancies, an additional program was conducted in the Vacuum Tank during 1967. This report is written to give the results of that program and to show where the new data agrees or disagrees with previous data obtained in both model and field tests.

At the present time, it has not been possible to resolve the discrepancy between the High-Gravity and Vacuum Tank results, and this analysis is restricted to the data on the latter tank. A brief summary of the High-Gravity Tank results is given in Appendix C.

2. MODEL TEST RESULTS

2.1 Method of Modeling

The scaling described by Snay, Goertner, and Price (1952) and by Goertner (1956) was used for this study. As in the former work, corresponding model and prototype conditions were calculated for free-water explosions using experimental values of the first period bubble parameters--both model and prototype. The free-water case is used since it is assumed that if geometric and dynamic similarity hold for the model and prototype explosion remote from the bottom, it will also hold--to good approximation--upon introduction of corresponding bottoms, i.e., the false bottom in the test tank and real bottom in the prototype. Free-water explosions at test conditions identical to the model or prototype bottom shot (except for the absence of the bottom) are referred to as "control shots."

The criterion for similarity between model and prototype was that the three characteristic numbers $(gt^2/A_{\max})_c$, $(A_{\min}/A_{\max})_c$, and $(A_{\max}/d)_c$ (see, e.g., Snay, 1964) be the same for the model and prototype explosions, where:

* Strictly speaking the NOL High-Gravity Tank is a "variable gravity" vacuum tank mounted on a centrifuge, whereas the NOL Vacuum Tank is a stationary (one-g) vacuum tank. Additional information on these test facilities can be obtained from the references cited in the first paragraph of Appendices C and D, respectively.

r_{\max} = maximum bubble radius, ft

d = depth of explosion, ft

A_{\min} = theoretical value of the minimum bubble radius for a non-migrating bubble at the same hydrostatic pressure as the migrating one, ft

g = acceleration of gravity = 32.15 ft/sec²

T = first period of bubble oscillation, sec

subscript "c" indicates control shot.

Characteristic numbers $(gT^2/A_{\max})_c$, $(A_{\min}/A_{\max})_c$, and $(A_{\max}/d)_c$ can be thought of as measures of the buoyancy, amplitude of pulsation, and free-surface geometry during the first period of oscillation. The first number gives a measure of the ratio of gravity force to inertial reaction for a water particle; i.e., it is the inverse of the Froude number. The computations of the model control shot parameters are described in Appendix A. A sample calculation for the prototype is given in Section 3.1.

2.2 Bubble Migration Behavior

In the 1967 program of tests, three strings of shots were fired. On each string the depth of explosion and the water temperature were held constant while the air pressure was varied by small increments. Essentially, this amounted to holding the characteristic numbers $(A_{\min}/A_{\max})_c$ and $(A_{\max}/d)_c$ constant and increasing the inverse Froude number $(gT^2/A_{\max})_c$ so that along each string the bubble behavior varied slowly from "sticking," or remaining intact and pulsating on the bottom, to "strongly migrating," when the entire bubble pulled away from the bottom and then behaved similarly to an explosion in free water.

This transition from "sticking" to "strongly migrating" encompassed a complex sequence of changing bubble behavior which was qualitatively similar for each of the strings. The following list is an attempt to describe this sequence:

(a) The entire bubble stays on the bottom through all of its oscillations.

An example of this type of behavior is shown in Figure 1. As the bubble contracts to the first minimum, it distorts into an upper and lower portion connected by a narrow stem. These then coalesce as the bubble expands to its second maximum.

(b) The bubble splits into two or more parts. The lower portion remains on or near the bottom. Figure 2 shows an example where the bubble separated into

two major parts during the third cycle*. Figure 3 shows an example where the bubble appeared to shatter into four or more parts during the second contraction.

(c) The entire bubble moves away from the bottom while it is still oscillating. Examples of this behavior are shown in Figures 4 and 5.

(As evidenced by the photographs shown in Figure 5, a migrating bubble may subsequently split as it migrates to the surface. Such splitting has sometimes been observed also on free-water explosions in tanks. To our knowledge this type of bubble splitting has never been investigated.)

Farley and Snay (1968)** describe formation of the re-entrant type jet which forms at the bottom of a free-water bubble during first collapse in the presence of a strong pressure gradient due to gravity. With bottom explosions--when the entire bubble pulls away during the first contraction--a similar re-entrant jet often occurs.

In the tests reported here, the inside of the bubble could not be seen. Consequently, the occurrence of the jet and its impact with the upper surface had to be inferred from the discontinuous eruption of the upper surface which occurred at this instant. When this eruption occurred at the instant the bubble reached its minimum cross-section, the flow appeared similar to that observed at jet impact with free-water bubbles. These bubbles were classified as "strongly migrating" (see last paragraph on page 5).

2.3 Experimental Results

The migration behavior was classified by viewing the film records in motion. The following classifications were used for the bubble behavior observed in the Vacuum Tank model experiments:

- Sticking -- The entire bubble stays on the bottom through all of its oscillations.
- Splitting -- The bubble breaks into two or more parts. The lower portion remains on or near the bottom.
- Migrating -- The entire bubble moves away from the bottom while it is still oscillating.

Observations of the bubble migration behavior in the static tank are presented in Figure 6 as a function of the characteristic numbers $(gT^2/A_{\max})_c$ and $(A_{\min}/A_{\max})_c$

* For splitting and migrating bubbles, the terms "maximum" and "minimum" for the successive cycles of bubble oscillation become imprecise after the first minimum. They are used here to convey the impression of oscillation which one gets when viewing the films.

** Figure 1.1 and related discussion on page 1.

for control shots (no bottom) at the same test conditions. The dashed lines roughly indicate the regions of different behavior. A plot analogous to Figure 6, but in three dimensions as a function of $(gT^2/A_{\max})_c$, $(A_{\min}/A_{\max})_c$, and $(A_{\max}/d)_c$, revealed the unexpected invariance of this behavior classification with $(A_{\max}/d)_c$. However, the subsequent behavior of the "migrating" bubble does depend on $(A_{\max}/d)_c$. See, e.g., Figure 11.)

In addition to the qualitative evaluation of the bubble migration behavior, it was possible to acquire quantitative data on the size and displacement of the bubble in many cases. At maximum volume the bubble was approximately hemispherical and its volume calculated by numerical integration averaged 82% of the control shot volume.

Defining an equivalent maximum radius for the bottom shot, $(A_{\max})_{eq}$, as the radius of a hemisphere of equal volume, the average value of the ratio

$(A_{\max})_{eq}/(A_{\max})_c$ was given by

$$\frac{(A_{\max})_{eq}}{(A_{\max})_c} = 1.18 \quad (1)$$

The individual measurements of this ratio are plotted in Figure 7. (Note: $(2)^{1/3} = 1.26 = \frac{(A_{\max})_{eq}}{(A_{\max})_c}$ for a hemisphere of volume equal to the control shot.

Within the limits of experimental scatter, the size* and shape of the bubble at maximum volume appeared to be independent of the three characteristic numbers $(gT^2/A_{\max})_c$, $(A_{\min}/A_{\max})_c$, and $(A_{\max}/d)_c$. Individual measurements of the maximum bubble diameter $D_{\max}/(A_{\max})_c$, the height $H_{\max}/(A_{\max})_c$, and their ratio H_{\max}/D_{\max} are shown in Figures 8, 9, and 10. Average values are

$$\frac{D_{\max}}{(A_{\max})_c} = 2.36 \quad \frac{H_{\max}}{(A_{\max})_c} = 1.21 \quad \frac{H_{\max}}{D_{\max}} = 0.51 \quad (2)$$

The experimental data used to construct Figures 6 through 10 are tabulated in Tables 1 and 2. In Figures 7 through 10 it is not meant to imply any functional dependence on $(A_{\max}/gT^2)_c$; these plots are presented to exhibit the individual measurements.

It was observed that for some of the largest values of gT^2/A_{\max} (greatest buoyancy forces) the bubble motion resembled that of a gravity-migrating bubble in free water. For these "strongly migrating" bubbles, the phenomenon of jet impact described in Section 2.2 was observed to occur as the bubble reached its minimum

* Size relative to $(A_{\max})_c$.

volume. In photographs of "weakly migrating" bubbles, it was more difficult to distinguish jet impact; and, impact always occurred after the bubble had passed minimum volume. These observations of jet impact are plotted as a function of $(gT^2/A_{\max})_c$ and $(A_{\max}/d)_c$ in Figure 11*. They did not vary within the limited range of $(A_{\min}/A_{\max})_c$ used for these model tests ($0.065 \leq (A_{\min}/A_{\max})_c \leq 0.085$). However, it should be pointed out that $(A_{\min}/A_{\max})_c$ is often much larger for prototype bubbles.

Strongly migrating bubbles can also be identified by the behavior of the stem which develops between the bubble and the bottom as the bubble collapses. For strongly migrating bubbles, this stem pulls away from the bottom and turns inside out to form the upward moving jet. These differences in appearance of the stem as it collapses are sketched in Figure 12. Photographs of the intermediate case, where the stem connection to the bottom during the first contraction is vertically walled and collapses upon itself as the bubble separates from the bottom, were shown in Figure 4.

The time, T , to jet impact for the strongly migrating bubbles is listed in Table 3 along with the ratio, T/T_c , to the corresponding free-water control. Since T is analogous to the first bubble period of the migrating bubble from a free-water explosion, it will also be referred to as the first bubble period and the same symbol will be used to designate it. The ratio, T/T_c , did not vary over the range of these tests. Its average value was

$$\frac{T}{T_c} = 1.14 \quad (3)$$

which is near the center of the range of the data listed by Murray et al (1961, Figure 16), for prototype explosions on various types of cratering bottoms.

The upward displacement, δ , of the strongly migrating bubbles at time, T , (first period migration) is compared with that observed for controls (free water) in Figures 13 and 14. Figure 13 shows data for the 1-foot model depth; Figure 14,

* Figure 11 gives a breakdown into two classifications of the observations of migrating bubbles indicated in Figure 6. To understand the interrelation between these two figures, it is necessary to visualize a three dimensional space with coordinates $(gT^2/A_{\max})_c$, $(A_{\max}/d)_c$ and $(A_{\min}/A_{\max})_c$. In this space, Figure 6 is then the projection on the $(gT^2/A_{\max})_c$, $(A_{\min}/A_{\max})_c$ plane--without distinction as to type of migrating bubble behavior. And, Figure 11 is the projection of migrating bubble data points on the $(gT^2/A_{\max})_c$, $(A_{\max}/d)_c$ plane using different symbols for the two types of migrating bubble behavior. The dashed lines in Figure 6 are thus projections of planes parallel to the $(A_{\max}/d)_c$ axis, while the dashed line in Figure 11 is the projection of a plane parallel to the $(A_{\min}/A_{\max})_c$ axis.

for the 2-foot model depth. The curves are previous free-water results reported by Goertner (1956), and the circles are the individual measurements from the controls fired on this test program. The control shot data from these two test programs are in agreement at the 1-foot model depth but differ by about 10% at the 2-foot model depth*.

The figures show that the first period migration for these strongly migrating bottom shots is greater than that of corresponding shots at the same test conditions with no bottom. This increase is about 20% for the bubble center and about 10 to 15% for the point of impact at the top of the bubble.

There are too few data to draw any but tentative conclusions for strongly migrating bottom shots. Goertner (1956) found for free-water explosions in the Vacuum Tank that the migration of the top was dependent on all three characteristic numbers-- $(gT^2/A_{\max})_c$, $(A_{\min}/A_{\max})_c$, and $(A_{\max}/d)_c$ --while the migration of the center could be described in terms of $(gT^2/A_{\max})_c$ and $(A_{\max}/d)_c$ alone. The limited data shown in Figures 13 and 14 indicate that this may also be true for strongly migrating bottom shots.

Measurements of the bubble diameter at the time of jet impact showed the reduced diameter $D_{\min}/(A_{\max})_c$ to be a function of both $(gT^2/A_{\max})_c$ and $(A_{\min}/A_{\max})_c$. No dependence on $(A_{\max}/d)_c$ was noted, but this may be due to the paucity of data. The data are roughly grouped about two distinct values of $(A_{\min}/A_{\max})_c$. These data are plotted in Figure 15.

3. COMPARISON WITH PROTOTYPE DATA

3.1 Equations for Comparing Model and Prototype Data

Since the results have been presented in terms of characteristic numbers for corresponding free-water explosions (controls) in the tanks, it is necessary to calculate the characteristic numbers $(gT^2/A_{\max})_c$, $(A_{\min}/A_{\max})_c$, and $(A_{\max}/d)_c$ for field prototypes in order to apply these results to particular full-scale explosion geometries. To do this, we use the empirical relations for the first period bubble parameters A_{\max} , T , and A_{\min}/A_{\max} :

* The reason for this discrepancy is not known. Possibly, there is significant interaction between the explosion and the front and back viewing windows at model depths of about two feet or greater. For the earlier tests, a lucite rather than plate glass rear window was used.

$$A_{\max} = J_{\infty} \left(\frac{W}{Z} \right)^{1/3} \quad (4)$$

$$T = K_{\infty} \frac{W^{1/3}}{Z^{5/6}} \left(1 - 0.1 \frac{A_{\max}}{d} \right) \quad (5)$$

$$\frac{A_{\min}}{A_{\max}} = N Z^{1/3} \quad (6)$$

where: W = charge weight, lb
 d = depth of explosion, ft
 $Z = d + 33$ = hydrostatic pressure at depth of explosion, ft of sea water
 J_{∞} = maximum radius coefficient in infinite water
 K_{∞} = period coefficient in infinite water
 N = minimum radius coefficient.

For simplification, we have assumed that the prototype explosion is a high explosive (HE) charge in sea water at one standard atmosphere air pressure. For other prototype explosions--e.g., nuclear explosions or explosions in fresh water--consult Snay (1964), Chapter VIII*. Sea water values for J_{∞} , K_{∞} , and N for several typical prototype explosives are listed below in Table 4.

TABLE 4

COE PROTOTYPE BUBBLE PARAMETERS**
 (Sea Water)

	J_{∞}	K_{∞}	N
TNT	12.6	4.36	0.023
Pentolite	12.6	4.36	0.022
HBX-1	14.4	4.97	0.025
HBX-3	15.6	5.41	0.029

* Equation 8.14, Snay (1964) contains a misprint. It should read

$$A_{\max}/A_{\min} = (N \cdot Z^{1/3})^{-1}$$

** TNT values for K_{∞} and J_{∞} are from Figure B-4, Holland, Caudle, and Goertner, 1967. K_{∞} and J_{∞} values for other explosives were calculated from values for $(RBE)_{TNT}$ listed in Figure B-2 of the same report. (The J_{∞} value for HBX-3 calculated using this method is probably about 4% high due to the high aluminum content of this explosive.) Values for N were taken from Table VI, Snay, et al, 1952.

To illustrate the utilization and some of the limitations of these model results, a numerical example will be given.

100-lb TNT Charge at 30-ft Depth. Using equations 4, 5, and 6 and the coefficients listed in Table 4, the following values are calculated:

$$(A_{\max})_c = 14.7 \text{ ft} \quad T_c = 0.609 \text{ sec} \quad \left(\frac{A_{\min}}{A_{\max}} \right)_c = 0.092$$

From these values, the characteristic numbers for the prototype control shot are then calculated:

$$\left(\frac{gT^2}{A_{\max}} \right)_c = 0.81 \quad \left(\frac{A_{\min}}{A_{\max}} \right)_c = 0.09 \quad \left(\frac{A_{\max}}{d} \right)_c = 0.49$$

Using these values in Figure 6, it is predicted that the bubble would migrate upward from a non-cratering bottom. From Equations (2), its height and diameter at maximum volume can be calculated. Using Figure 11, it is uncertain whether or not jet impact would be observed. If impact does occur, the upward displacement of the bubble at time of impact will be 10 to 20% greater than for an explosion in free water.

3.2 Comparison with Prototype Data for Cratering Bottoms

As mentioned previously, three experimental studies have been done of bubble behavior from bottom explosions of high explosive (HE) charges; namely, those of Snay (1953); Murray, Santamaria, and Clifford (1961); and Young (1968). For each of these studies, the primary source of data was full-scale HE explosions on various cratering bottoms.

An approximate synthesis of much of the existing HE explosion bubble data was reported by Murray, et al, in 1961. For bottom explosions, they estimated that over the reduced depth range*

* For describing bubble phenomena from prototype explosions, the reduced depth $(Z/A_{\max})_c$ is approximately proportional to the Froude Number. The characteristic number $(gT^2/A_{\max})_c$ for the prototype is related to $(Z/A_{\max})_c$ by

$$\frac{gT^2}{A_{\max}} = \left[\frac{gK_{L,2}}{J_0} \left(1 - 0.1 \frac{A_{\max}}{d} \right)^2 \right] \left(\frac{Z}{A_{\max}} \right)^{-1}$$

(derived from Equations 4 and 5). In many prototype studies the bracketed expression is treated as a constant.

$$3.5 \leq (Z/A_{\max})_c \leq 7.0 \quad (7)$$

the bubble splits "into two parts, both of which may migrate upwards." At shallower depths, the migration is roughly similar to that in free water and, at greater depths, the bubble sticks to the bottom.

Young (1968) presented an analysis of the upward transport of explosion products and surrounding water by underwater explosions. He described and classified the surface eruptions as a function of the charge weight and the depth of explosion for both deep-water and bottom explosions (Young, 1968, Figures 2.7 and 2.9). His data for bottom explosions showed that when the reduced depth $(Z/A_{\max})_c$ reaches approximately 7.4, the radial plumes characteristic of deep explosions no longer occur, and only a water mound appears. At $(Z/A_{\max})_c \approx 12.5$, the mound ceases to occur for the bottom explosions and only an upwelling occurs*. From the evidence presented by Snay, by Murray et al, and also in this report, it is plausible to assume that these transitions reported by Young correspond to the transitions in bottom-shot bubble behavior termed splitting and sticking--even though, this range of reduced depths differs from that given by Murray et al (1961).

The strongest evidence of bubble splitting in these field programs was the observation of a well-developed set of plumes, followed a few seconds later by an upwelling of a large volume of small bubbles, on two 1200-pound HBX-1 bottom shots in 85 and 110 feet of water (Murray, et al, 1961). Also, an 1110-pound HBX-1 shot at a depth of 140 feet showed evidence of a second bubble emerge about 7.5 seconds after the shot (Young, 1968). The latter was an actual upheaval of the surface, while the phenomenon reported by Murray et al, could conceivably contain bubbles of natural gases released from the bottom.

Figure 16 shows individual data points from prototype bottom shots which provide evidence of the influence of the bottom on bubble phenomena. It is not possible to draw positive conclusions from this figure. However, there is some qualitative consistency; e.g., the points indicated by the symbols "□" and "▽" seem to be reliable evidence of splitting and sticking, respectively. Additional field data, with more complete documentation of bubble behavior, is needed before the similarities and differences between prototype data on cratering bottoms and tank data on a rigid bottom can be fully evaluated.

* The conversion to the parameter $(Z/A_{\max})_c$ from the dimensionless parameter $(A_{\max}/d)_c$ employed by Young to describe the surface eruption was calculated for a 200-lb TNT charge weight, which is about mid-range for the bottom shot data reported by Young.

Figure 17 compares with the model test results the estimated ranges for the occurrence of bubble splitting as predicted by Murray et al (1961) and Young (1968). The prototype behavior is indicated by two adjacent arbitrary-width bands whose centerline is the curve for a 1200-lb HBX-1 charge at variable depth in the sea*. Taken together, these estimates for prototype bubbles predict bubble splitting at values of the inverse Froude number equal to or greater than that observed in the model tests. Since the model bubbles oscillated more strongly (smaller $(A_{\min}/A_{\max})_c$), this suggests that, other things being equal, there is more tendency for the bubble to stick to a cratering than to a non-cratering bottom.

3.3 Observations of Enhanced Migration and Jetting

Young (1968, page 24) reported an unexpected result from field tests with 10,000-pound HBX-1 charges. These charges, when fired at a depth of 125 feet in water 150 feet deep (three shots), produced plumes two to three times as high as similar charges at the same depth in deep water. For these explosions

$$\left(\frac{Z}{A_{\max}}\right)_c = 2.8$$

$$\left(\frac{gT^2}{A_{\max}}\right)_c = 1.4$$

This condition falls in the region of expected migration as shown in Figure 16 and almost certainly results in a strongly migrating bubble. Thus, Young's result would appear related to the enhanced bubble migration for strongly migrating bubbles observed in the present model experiments (Figures 13 and 14).

Sherman (1965) provided another observation of enhanced migration in the presence of a bottom. He fired 0.2-gram lead azide charges in the NOL High-Gravity Tank in contact with an aluminum plate and compared the trajectories of the upper surface with those of control shots. For the shallower shots, those with $(gT^2/A_{\max})_c \geq 0.7$, the upward displacement of the bubble top at time of jet impact averaged some 20% greater for the bottom shots than for the controls. His plots also showed that the initial velocity of the upper surface after impact was greater for these bottom shots than for the control shots. Due to the problems pointed out in Appendix C of this report, these High-Gravity Tank results are tentative at best. Nevertheless, they, too, point to the existence of enhanced gravity migration effects in the presence of a bottom under certain--as yet to be defined--conditions.

* The centerline was calculated using equations 4, 6, and the footnote on page 9.

4. SUMMARY OF RESULTS

(a) The following succession of bubble behaviors was observed as the inverse Froude number $(gT^2/A_{\max})_c$ increased:

- The bubble remained intact and pulsated on the bottom.
- The bubble split into two or more parts and the lower portion remained on or near the bottom.
- The bubble rose directly to the surface. Jet impact occurred as the bubble expanded after the first minimum.
- The bubble rose directly to the surface. Jet impact occurred at the instant of minimum bubble volume.

The tendency to stick depended on the amplitude of oscillation $(A_{\min}/A_{\max})_c$ as well as the inverse Froude number $(gT^2/A_{\max})_c$. The subsequent upward motion of the migrating bubbles--in particular, the formation and impact of the bubble jet--depended also on the surface geometry $(A_{\max}/d)_c$.

(b) The first bubble minimum of the strongly migrating bottom explosions occurred some 10 to 20% higher from the point of explosion than for corresponding free-water explosions. Anomously high plume heights reported by Young (1968) for 10,000-pound near-bottom explosions indicate that such enhanced gravity migration may also occur on full-scale explosions.

(c) Present estimates from field tests for prototype bubble behavior on cratering bottoms give bubble sticking at about the same or greater values of the inverse Froude number $(gT^2/A_{\max})_c$ than observed with more strongly oscillating model bubbles on a non-cratering bottom. This suggests that there is more tendency to stick to a cratering bottom than to a non-cratering bottom.

5. CONCLUSIONS AND RECOMMENDATIONS

It is not clear at the present time what the effect of a bottom would be on a deep nuclear explosion. It should be emphasized that the data presented here are for gas bubbles produced by conventional explosives, and the applicability of the results to nuclear explosions is doubtful. However, the data can be extremely useful in planning field test with steam-generating explosives, such as Lithanol (Young, 1968), or model tests with sparks or exploding wires. Such tests can be expected to provide information for nuclear predictions.

It would appear crucial to determine the role of cratering in retarding bubble migration. Therefore, a similar Vacuum Tank study of bubble behavior on a cratering bottom should be carried out.

In addition, work should be directed toward similar tests on cratering and non-cratering bottoms in the High-Gravity Tank so that the dependence on oscillation amplitude, $(A_{\min}/A_{\max})_c$, can be studied at hydrostatic pressures comparable to those on field tests. Only in the High Gravity Tank can such small scale underwater tests be carried out without encountering the uncertainties introduced by boiling (discussed in Appendix B).

Enhancement of bubble migration (and jetting) due to bottom proximity has important implications in regard to ship damage. This study indicates that such enhancement does occur, both in model and full-scale tests. Evidence of significant retardation due to bottom proximity has also been reported (Paragraph 7.12, Snay, 1953). This problem, apart from whether outright sticking or splitting occurs, requires further study by both model and full-scale experiments.

REFERENCES

- Bartlett, R. W., 1965, "Scaling of Some Large Underwater Explosions in an Accelerated Test Tank", NOLTR 65-13, Secret
- Cole, R. H., 1948, "Underwater Explosions", Princeton University Press, Unclassified
- Farley, T. E. and Snay, H. G., 1968, "A Simplified Analysis of the Bubble Jet Pulse", NOLTR 6842, Unclassified
- Goertner, J. F., 1956, "Vacuum Tank Studies of Gravity Migration of Underwater Explosion Bubbles", NAVORD Report 3902, Confidential
- Goertner, J. F., 1968, "Error Analysis for Vacuum Tank Modeling of Underwater Explosion Bubbles", NOLTR 8045, Unclassified*
- Holland, N. O., Caudle, K. F. and Goertner, J. A., 1967, "Explosives--Effects and Properties", NOLTR 65-218, Confidential
- Murray, W. W., Santamaria, R. M. and Clifford, N., 1961, "Engineering Estimates of the Behavior of the Gas Bubble Produced by an Underwater Explosion", DTMB Report C-1319, Confidential
- Price, R. S., Zuke, W. G. and Infantino, C., 1964, "A Study of Underwater Explosions in a High Gravity Tank", NOLTR 63-125, Confidential
- Sherman, P. S., 1965, "VELA Bubble Containment Study in the NOL High Gravity Tank", NOLTR 6985, Unclassified*
- Sherman, P. S., 1968, "Deflection of NOL Vacuum Tank Windows", NOLTR 8002, Unclassified*
- Shiffman, M. and Friedman, B., 1944, "On the Best Location of a Mine Near the Sea Bed", published in Vol. II of "Underwater Explosion Research", Office of Naval Research, 1950, Unclassified
- Snay, H. G. and Christian, E. A., 1952, "Underwater Explosion Phenomena: The Parameters of a Non-Migrating Bubble Oscillating in an Incompressible Medium", NAVORD Report 2437, Unclassified
- Snay, H. G., Goertner, J. F. and Price, R. S., 1952, "Small Scale Experiments to Determine Migration of Explosion Gas Globes Towards Submarines", NAVORD Report 2280, Confidential
- Snay, H. G., 1953, "Optimum Mine Characteristics Part II--Damage Analysis", NAVORD Report 2786, Confidential
- Snay, H. G., 1964, "Model Tests and Scaling", NOLTR 63-257, Unclassified

* NOLTR's (Technical Notes) are not distributed outside the Laboratory. For additional information, contact the Underwater Explosions Division (Code 243) of the Naval Ordnance Laboratory.

NOLTR 68-207

Young, G. A., 1968, "The Transport of the Products of Very Deep Underwater Explosions", NOLTR 67-179, Confidential FRD

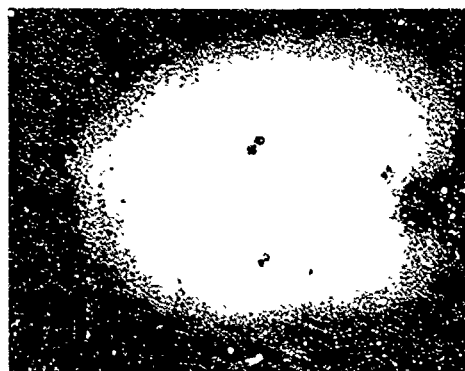
Zuke, W. G., 1960, "Laboratory Scaling of Underwater Nuclear Explosion Rubbles", NAVWEPS Report 6707, Confidential

Zuke, W. G., 1961, "Improved Small Charge and Charge Mounting for Use in Laboratory Underwater Explosion Experiments", NOLTN 5328, Unclassified*

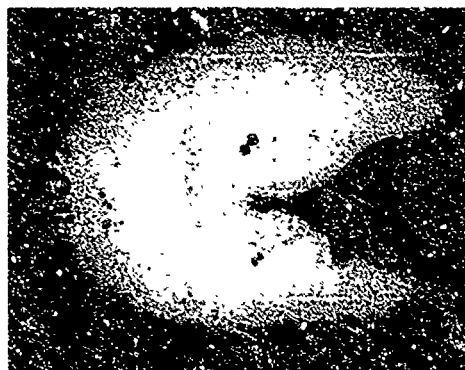
* NOLTN's (Technical Notes) are not distributed outside the Laboratory. For additional information, contact the Underwater Explosions Division (Code 243) of the Naval Ordnance Laboratory.



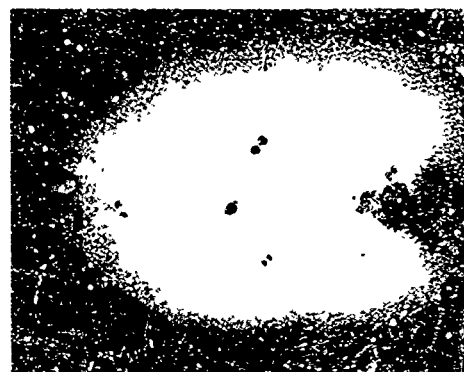
TIME (MSEC) = 26.9
1st MAXIMUM



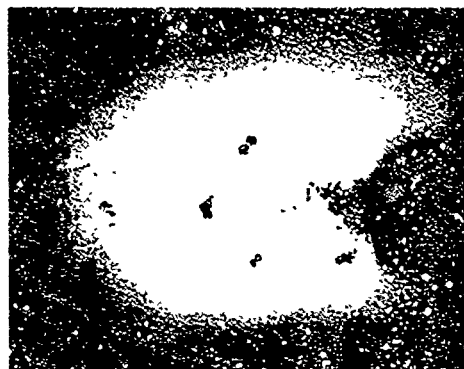
59.6
1st MINIMUM



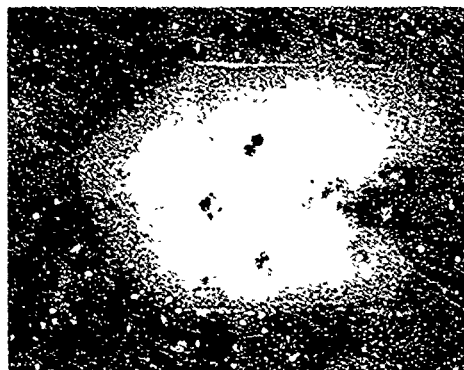
79.3
 \approx 2nd MAXIMUM



100.7
 \approx 2nd MINIMUM

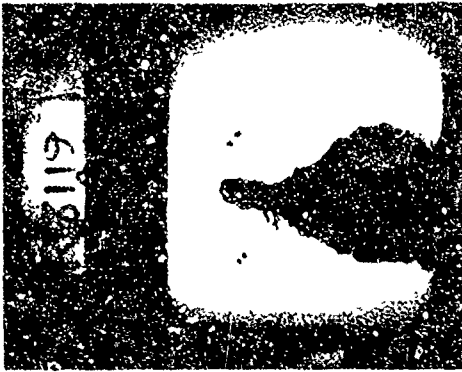


120.7
 \approx 3rd MAXIMUM

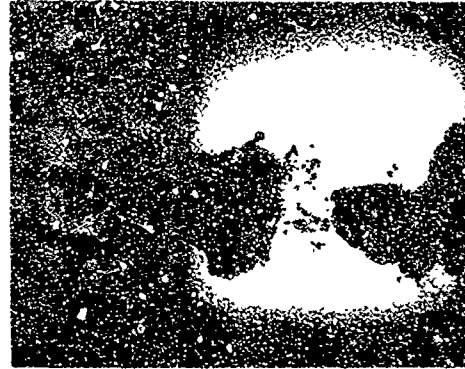


139.7
 \approx 3rd MINIMUM

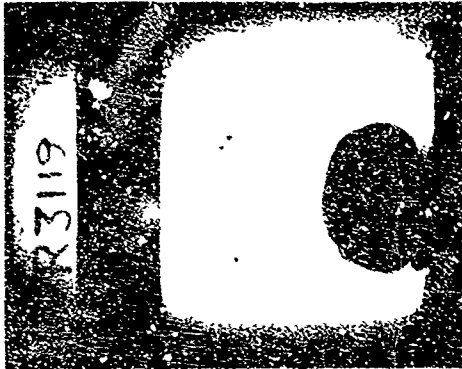
FIG. 1 STICKING BUBBLE



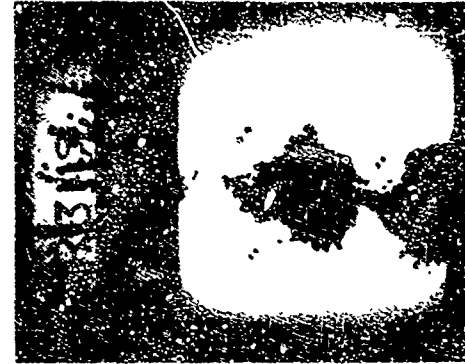
109.4
SLIGHTLY AFTER
2nd MAXIMUM



246.2



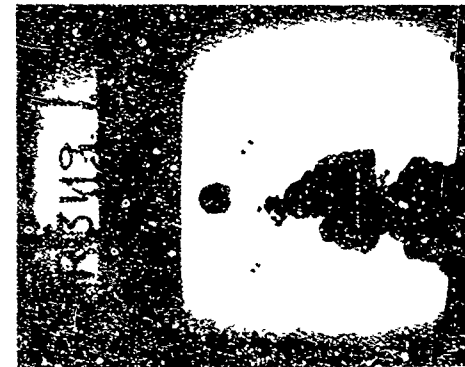
78.4
1st MINIMUM



158.4
≈ 3rd MAXIMUM

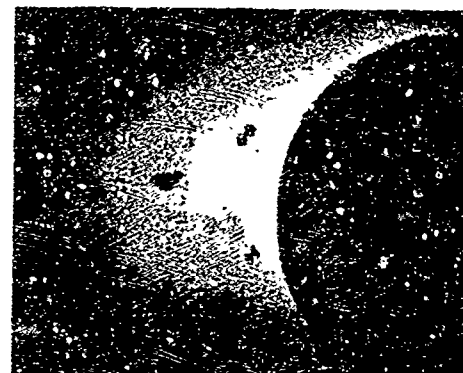


TIME (MSEC) = 37.8
1st MAXIMUM

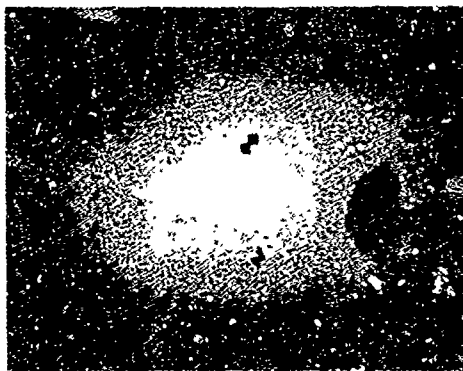


124.7
≈ 2nd MINIMUM
(BUBBLE SPLITTING)

FIG. 2 SPLITTING BUBBLE



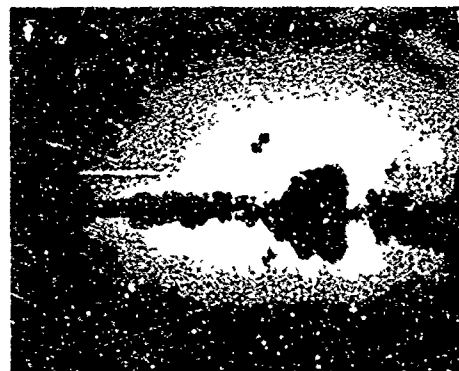
TIME (MSEC) = 49.8
1st MAXIMUM



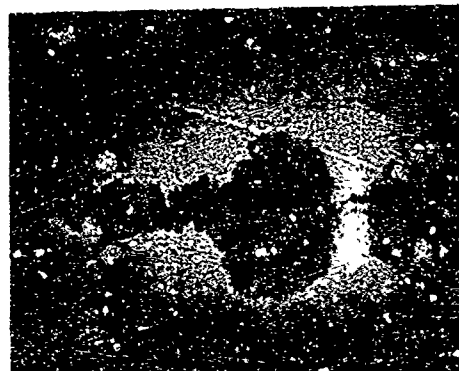
93.4
1st MINIMUM



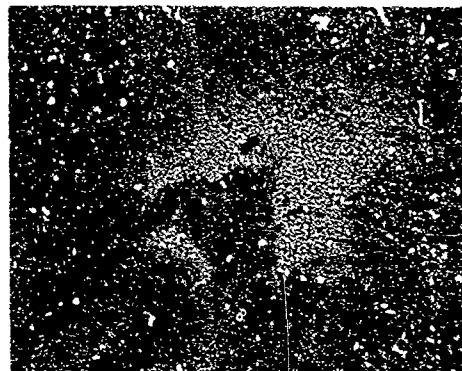
130.4
≈ 2nd MAXIMUM



155.7
≈ 2nd MINIMUM
BUBBLE SHATTERS



184.9
≈ 3rd MAXIMUM
UPPERMOST PORTION
OF BUBBLE VENTS



209.6
≈ 3rd MINIMUM

FIG. 3 SPLITTING BUBBLE

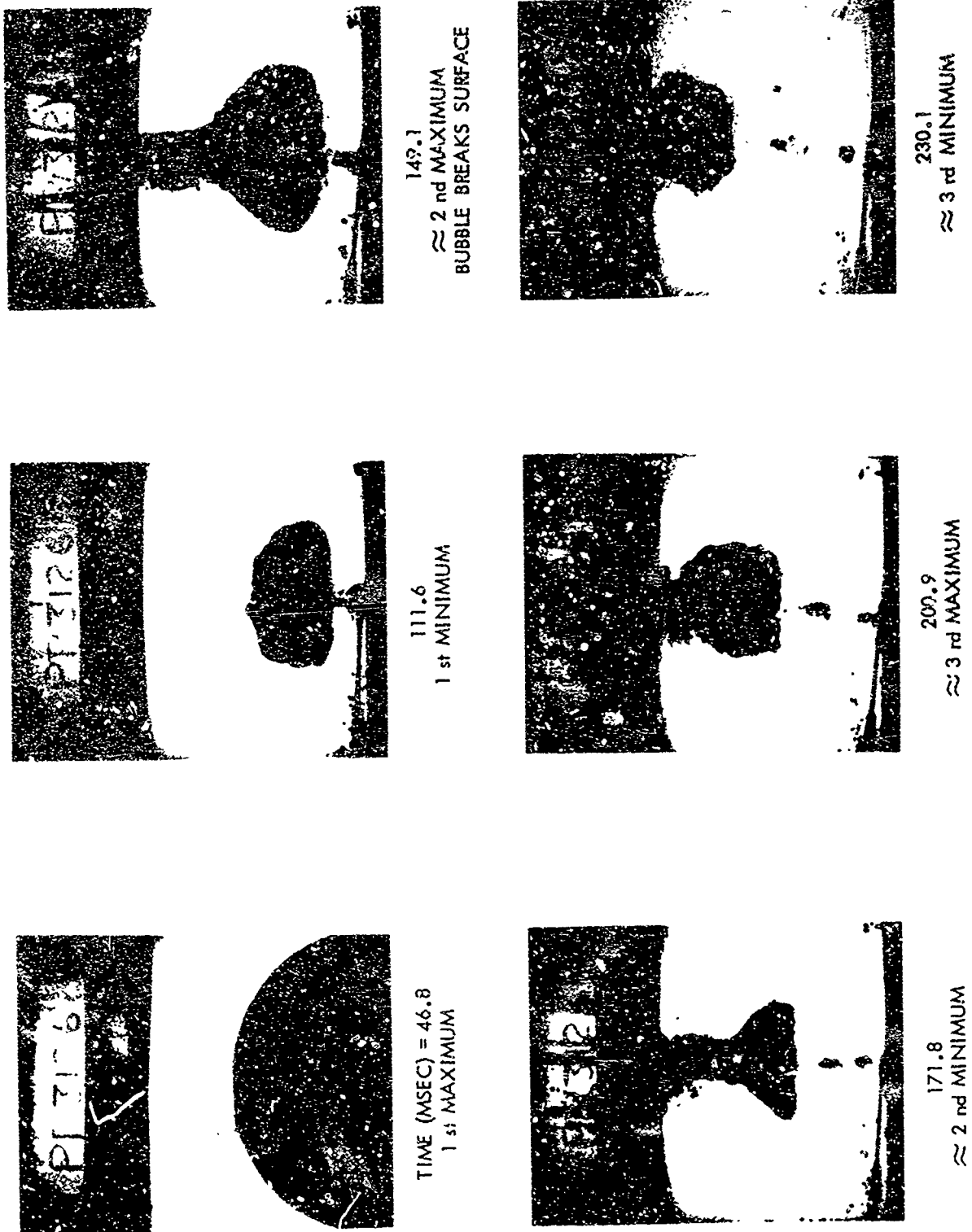


FIG. 4 WEAKLY MIGRATING BUBBLE (INTERMEDIATE CASE)



TIME (MSEC) = 62.4
1st MAXIMUM



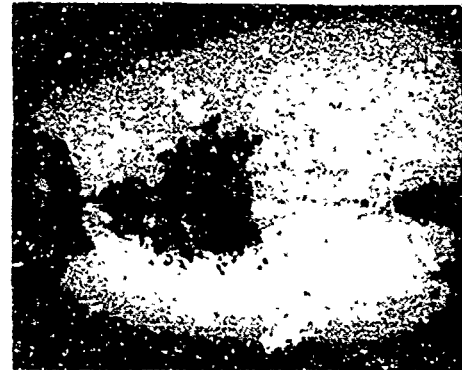
122.2
1st MINIMUM



166.6
 \approx 2nd MAXIMUM



203.9
 \approx 2nd MINIMUM
BUBBLE VENTS AND
PULLS APART



227.5
 \approx 3rd MAXIMUM

FIG. 5 STRONGLY MIGRATING BUBBLE

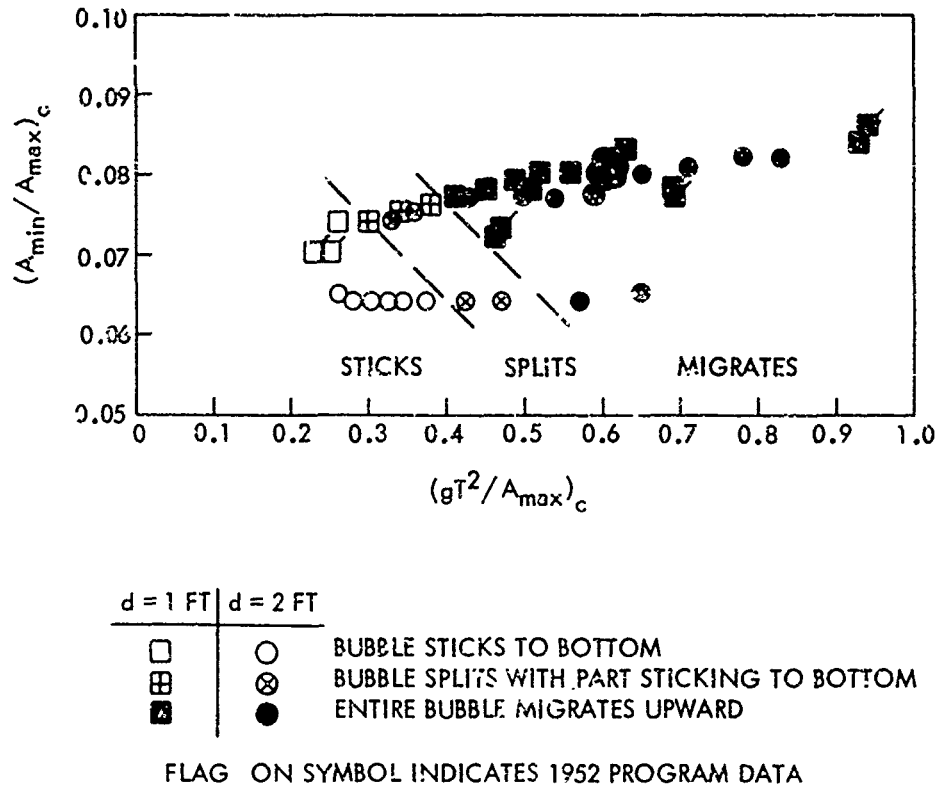


FIG. 6 BEHAVIOR OF BUBBLES ON NON-CRATERING BOTTOM AS A FUNCTION OF $(gT^2/A_{max})_c$ AND $(A_{min}/A_{max})_c$

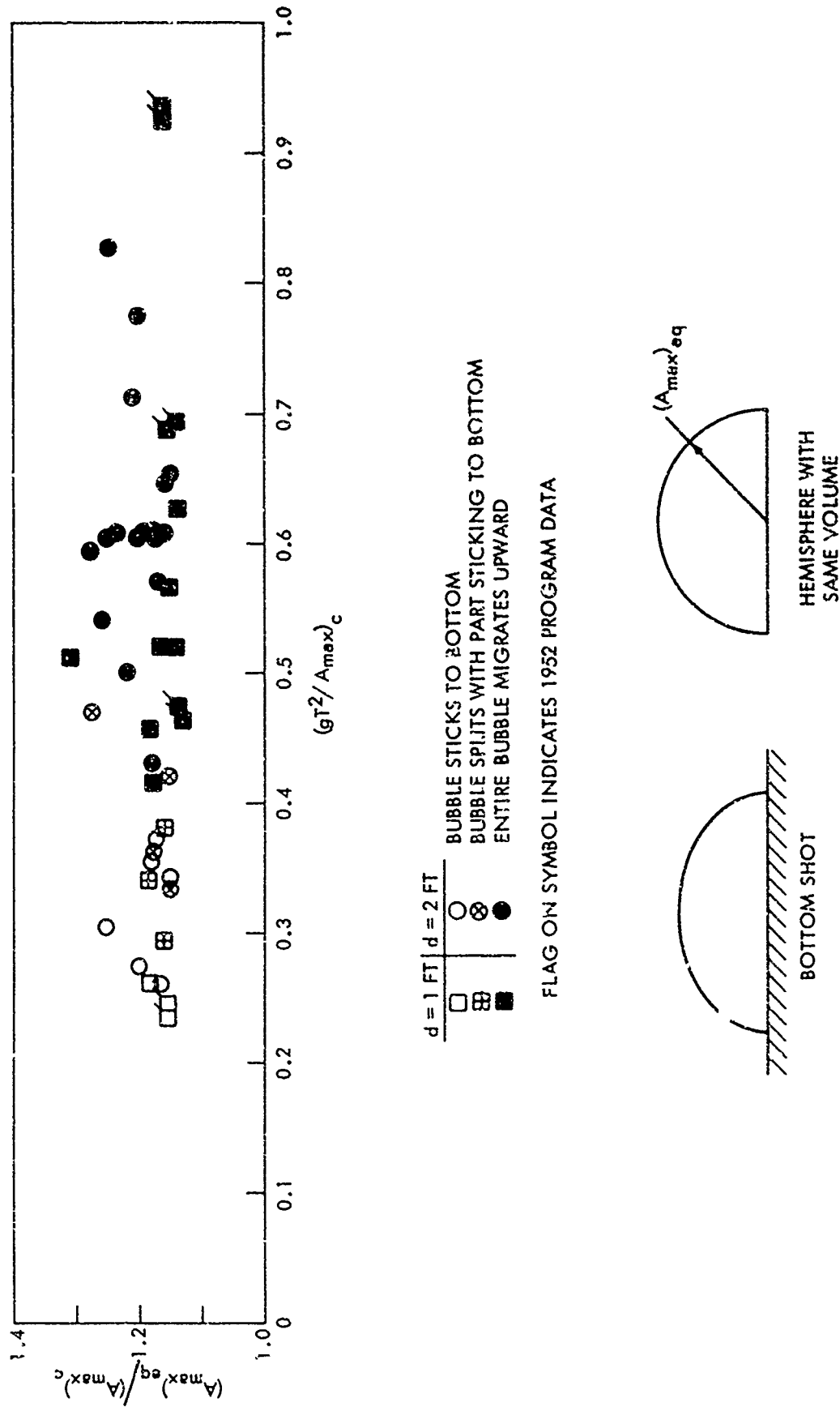
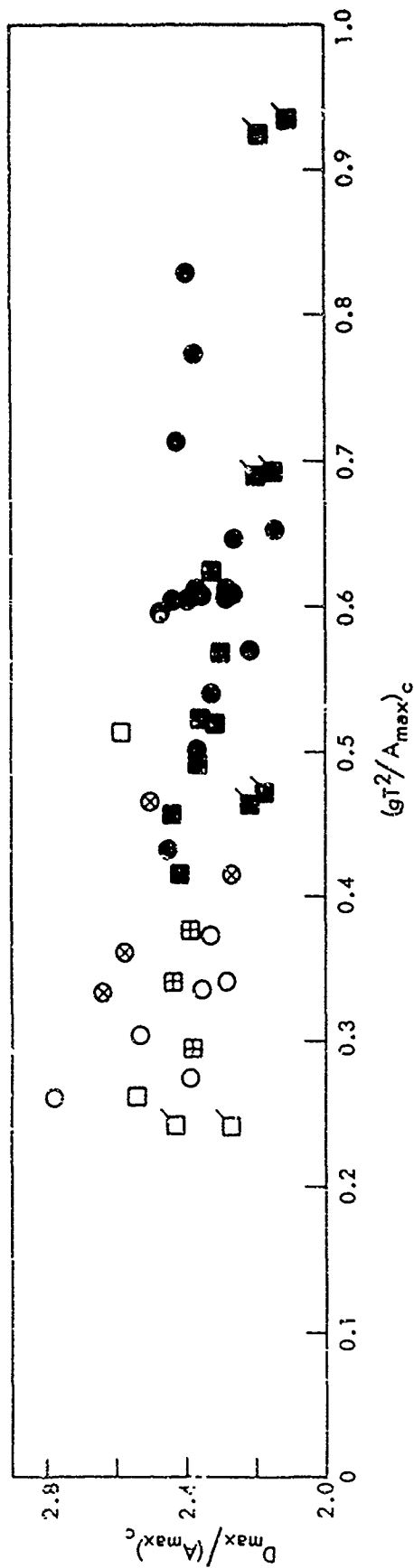


FIG. 7 REDUCED EQUIVALENT RADIUS $(A_{max}^{eq} / A_{max}^c)$ AT FIRST MAXIMUM — NON-CRATERING BOTTOM



FLAGS ON SYMBOL INDICATES 1952 PROGRAM DATA

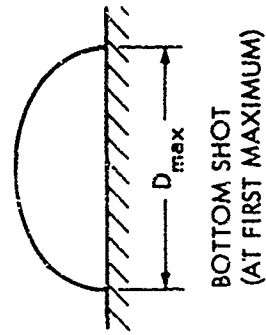


FIG. 8 REDUCED DIAMETER $D_{max}/(A_{max})^c$ AT FIRST MAXIMUM — NON-CRATERING BOTTOM

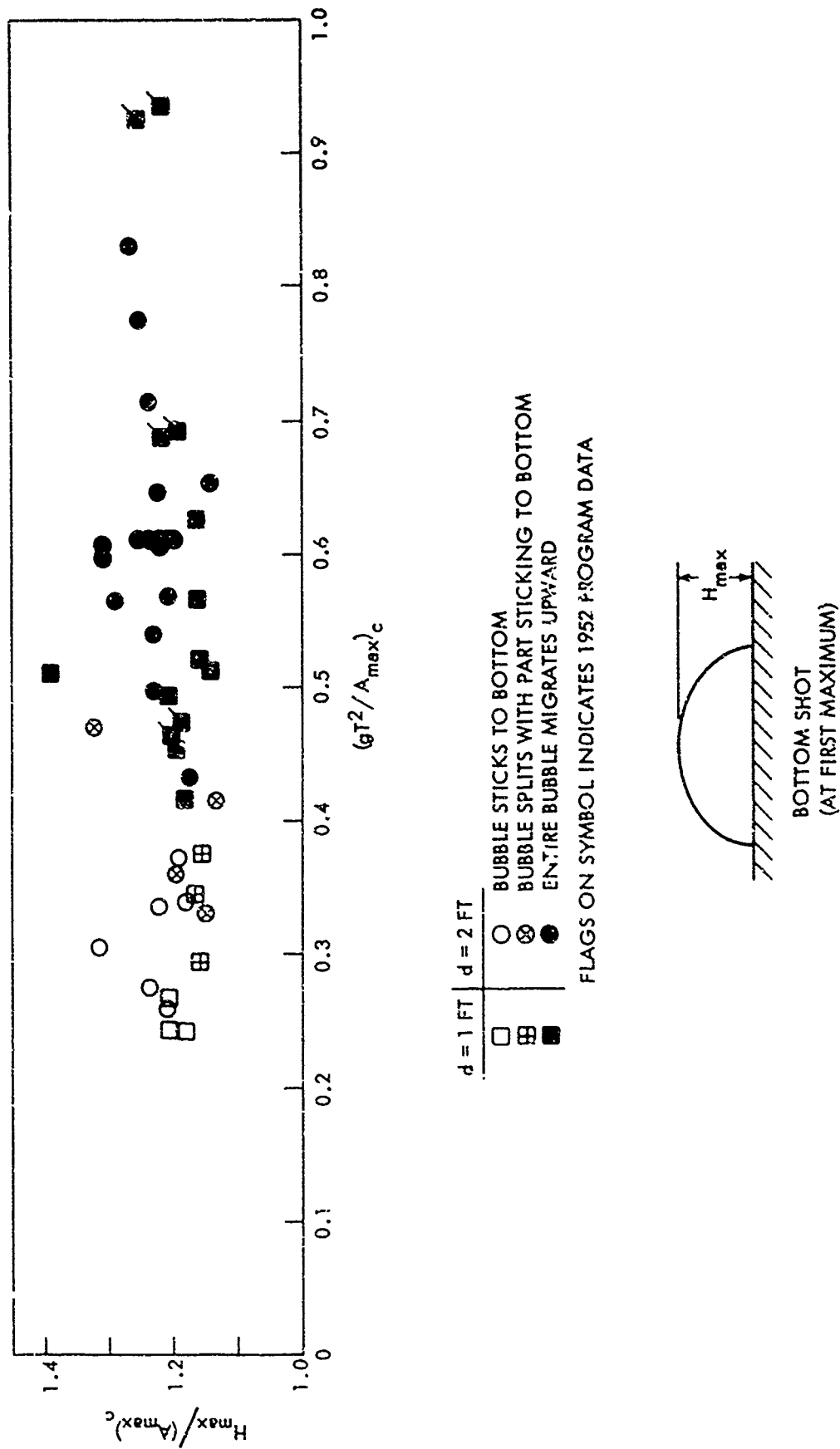


FIG. 9 REDUCED HEIGHT $H_{max}/(A_{max})^c$ AT FIRST MAXIMUM — NON-CRATERING BOTTOM

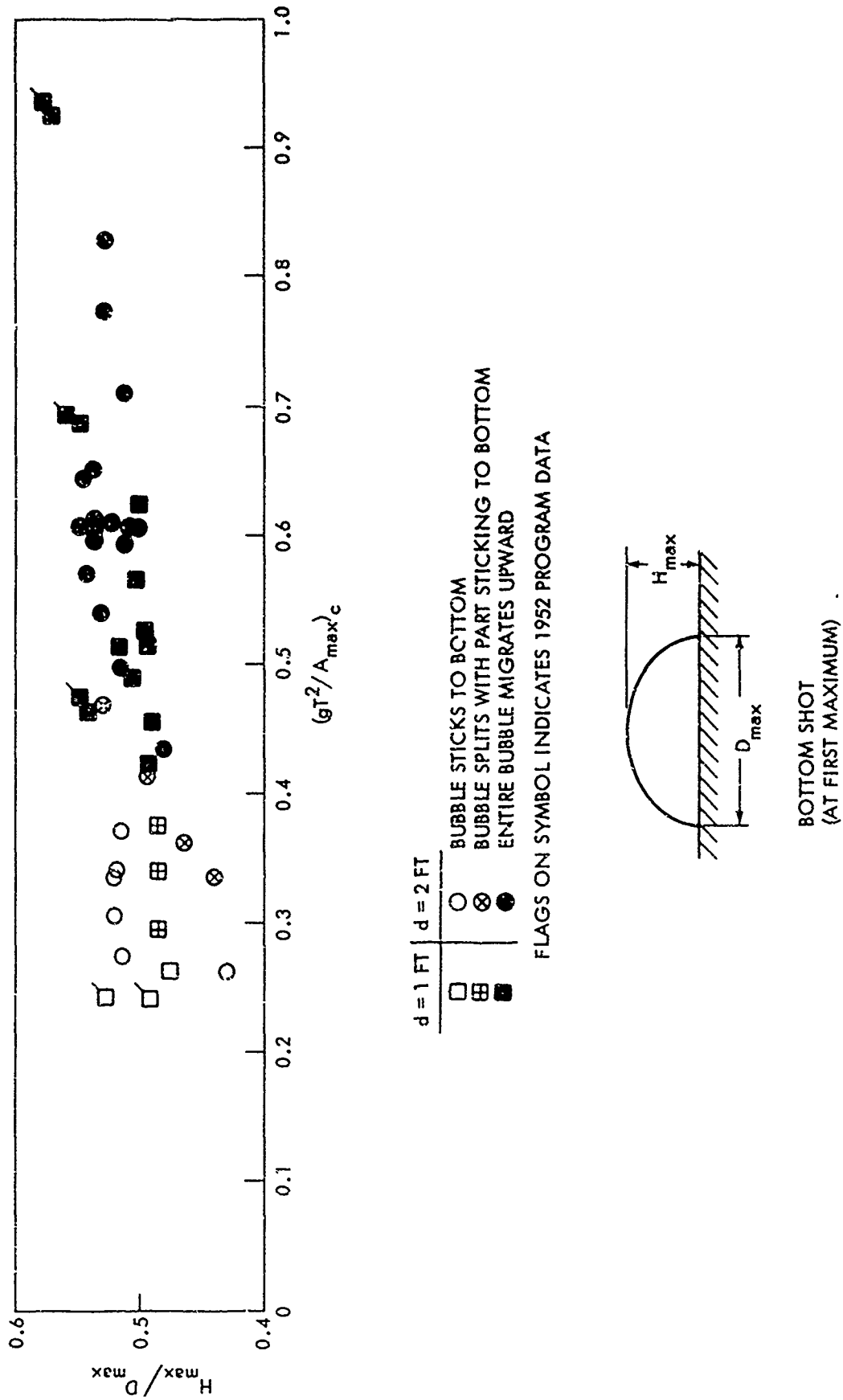


FIG. 10 HEIGHT-TO-DIAMETER RATIO H_{\max}/D_{\max} AT FIRST MAXIMUM — NON-CRATERING BOTTOM

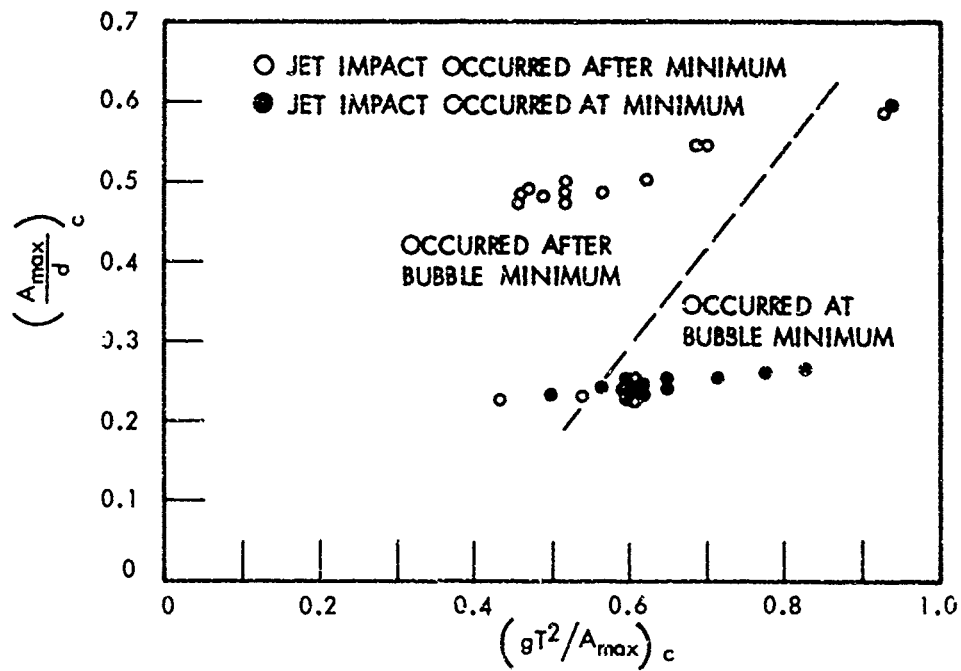


FIG. 11 OBSERVATIONS OF JET IMPACT FOR MIGRATING BUBBLES AS A FUNCTION OF $(gT^2/A_{max})_c$ AND $(A_{max}/d)_c$ -- NON-CRATERING BOTTOM

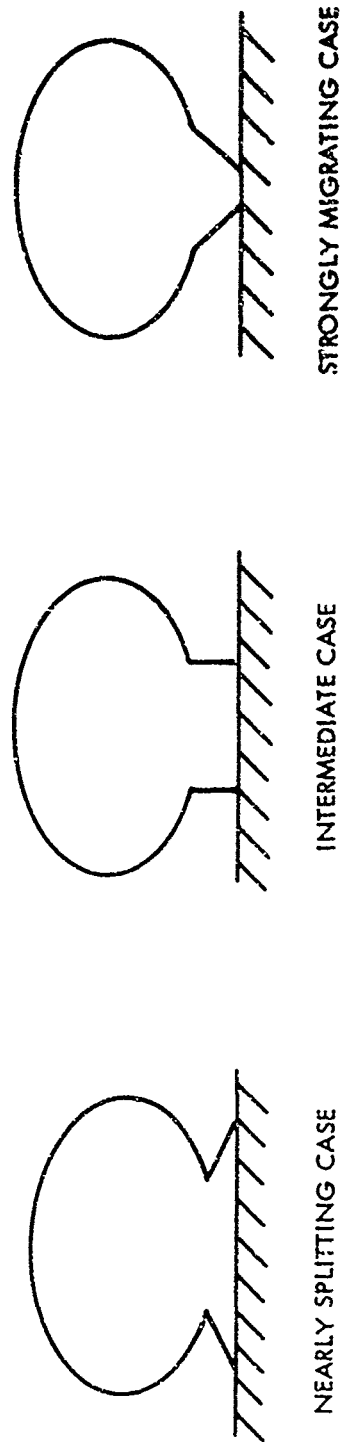


FIG. 12 DIFFERENT MIGRATING BUBBLE BEHAVIOR --- AT A TIME JUST BEFORE THE FIRST MINIMUM

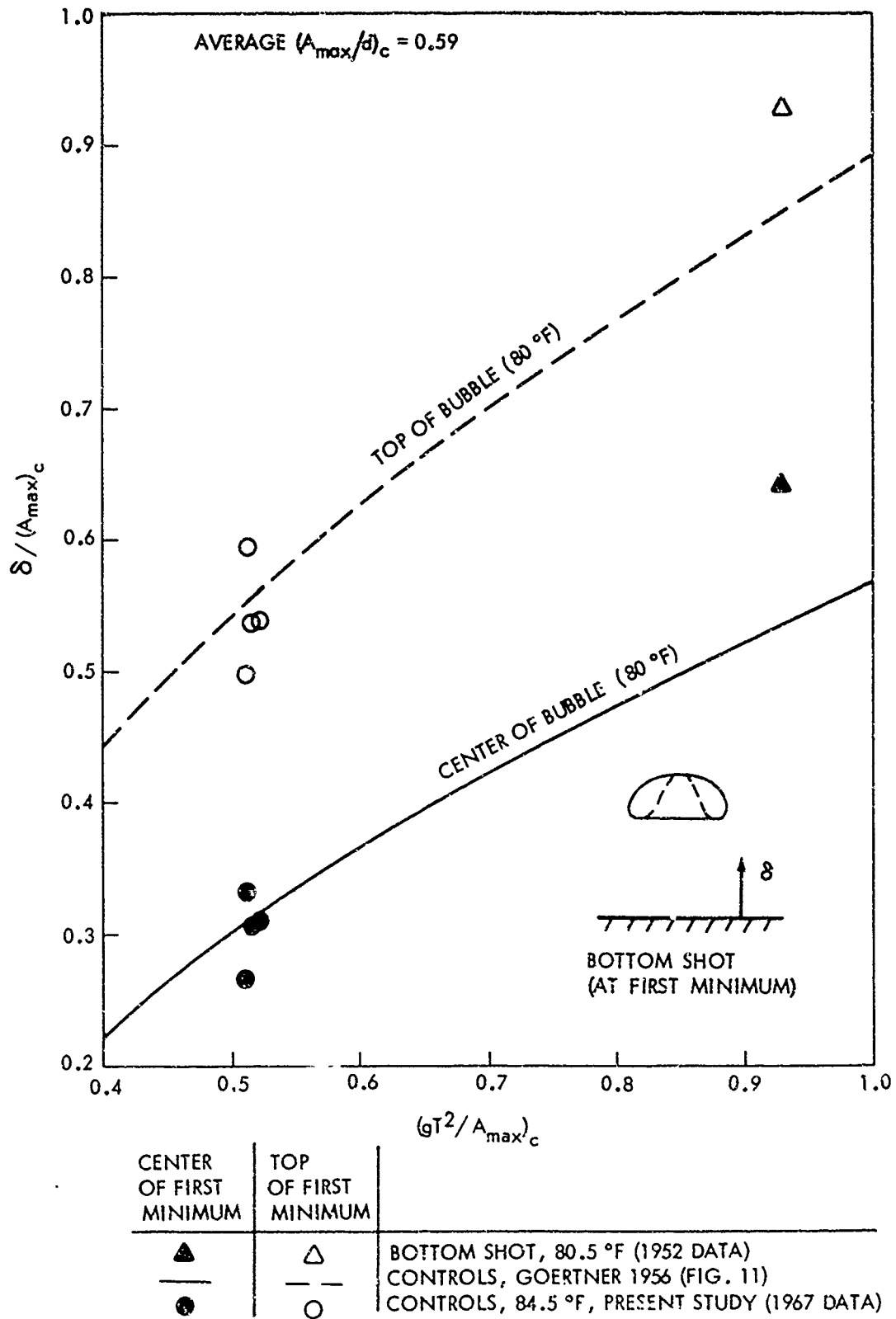


FIG. 13 COMPARISON OF REDUCED FIRST PERIOD BUBBLE MIGRATION WITH AND WITHOUT BOTTOM — STRONGLY MIGRATING CASE, $d = 1$ FT

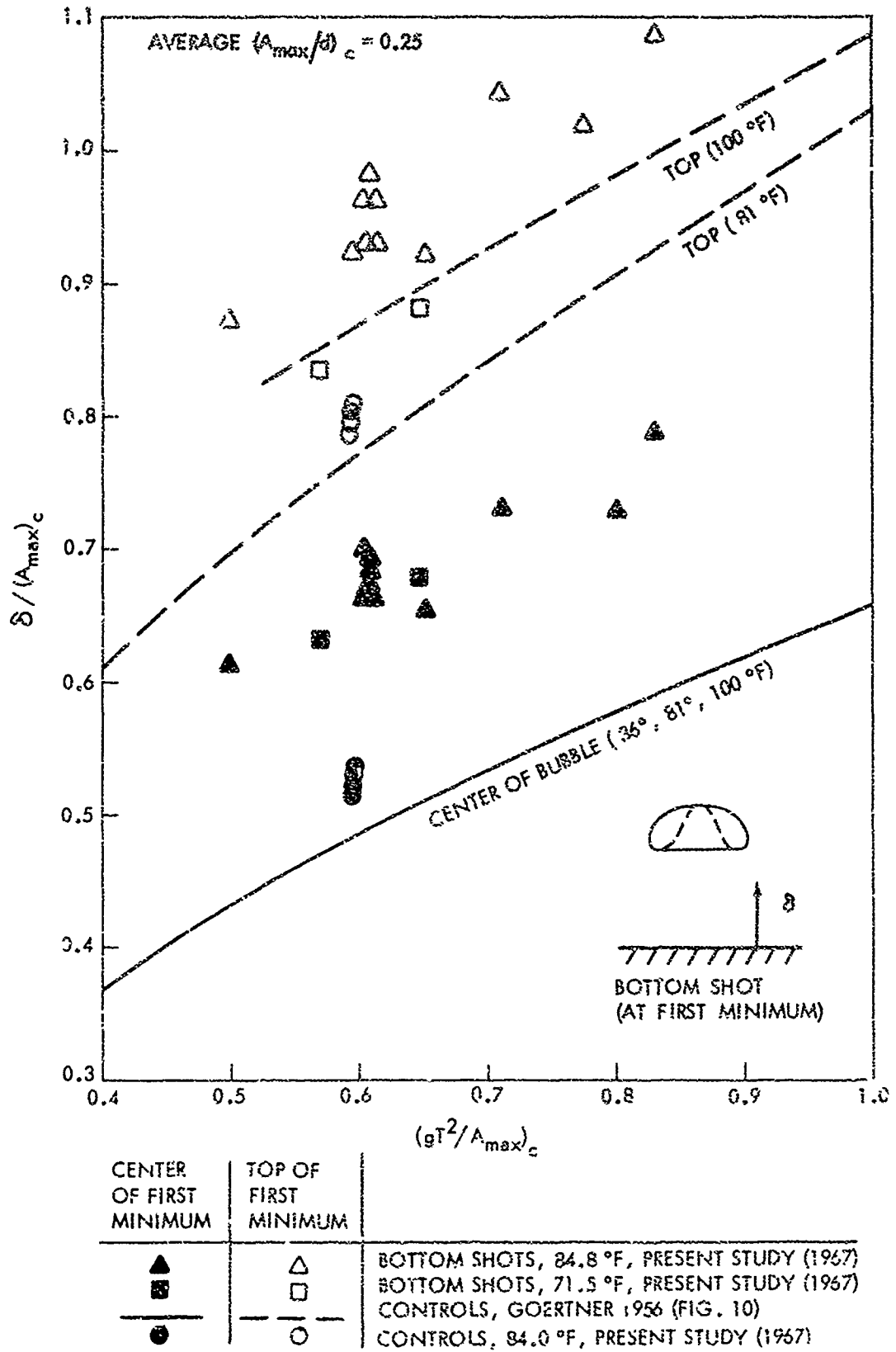
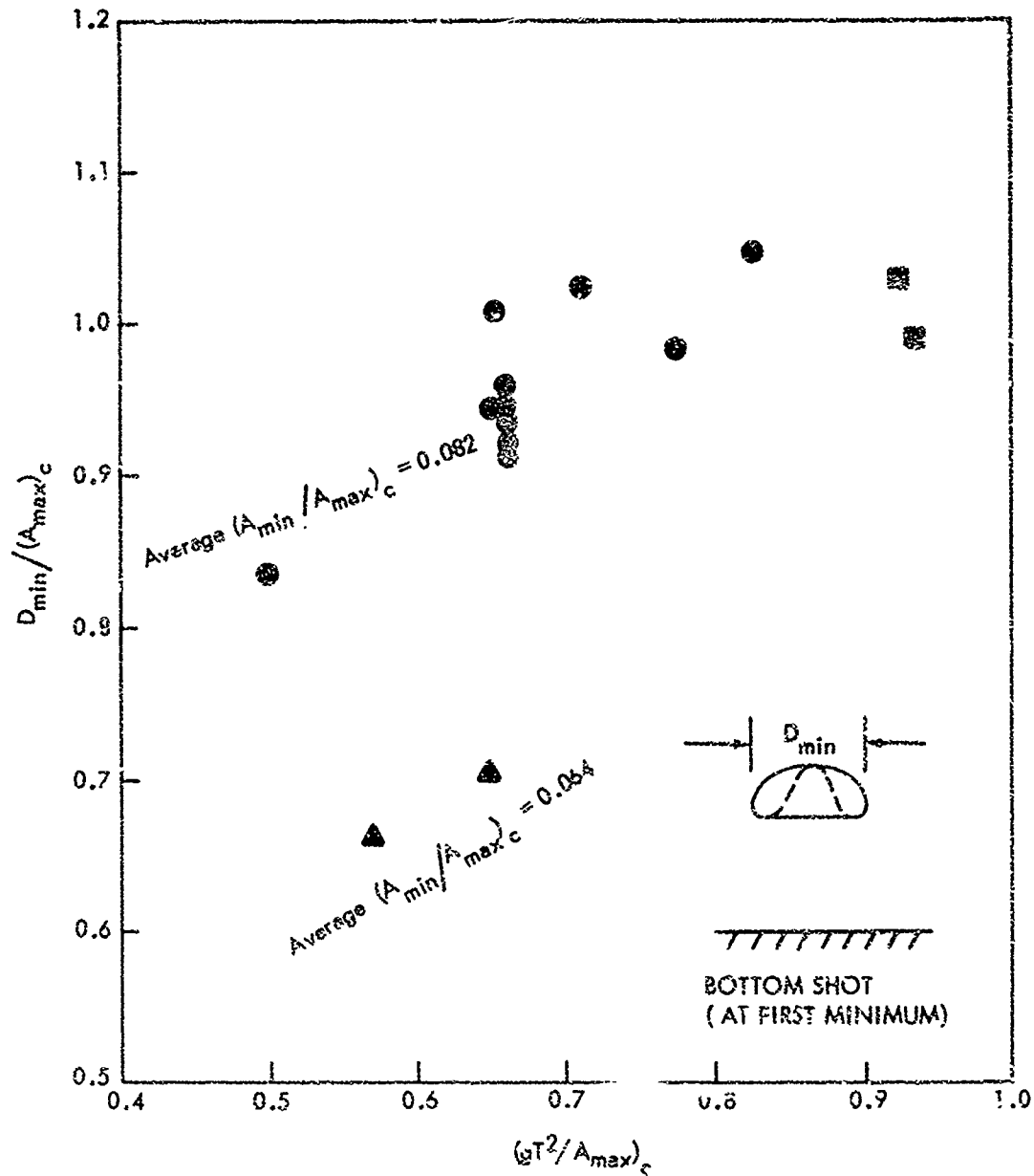


FIG. 14 COMPARISON OF REDUCED FIRST PERIOD BUBBLE MIGRATION WITH AND WITHOUT BOTTOM — STRONGLY MIGRATING CASE, $d = 2$ FT



- ▲ BOTTOM SHOTS, 71.5 °F, d = 2 FT, PRESENT STUDY (1967)
- BOTTOM SHOTS, 80.5 °F, d = 1 FT, 1952 DATA
- BOTTOM SHOTS, 84.8 °F, d = 2 FT, PRESENT STUDY (1967)

FIG. 15 REDUCED MINIMUM DIAMETER, $D_{min}/(A_{max})_c$ AS A FUNCTION OF $(gT^2/A_{max})_c$ AND $(A_{min}/A_{max})_c$ — STRONGLY MIGRATING CASE, NON-CRATERING BOTTOM

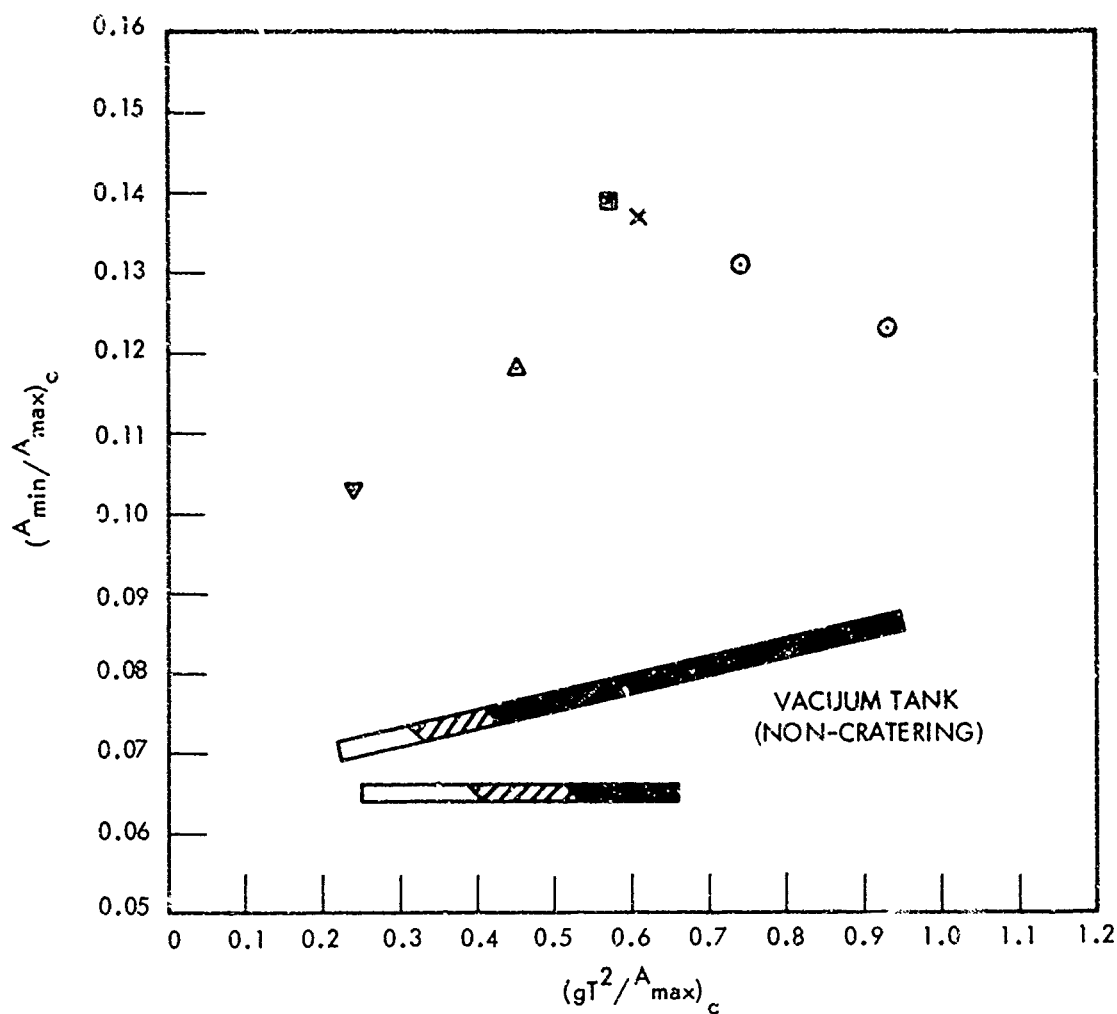


FIG. 16 COMPARISON OF NON-CRATERING MODEL BEHAVIOR WITH OBSERVATIONS FROM FULL SCALE TESTS

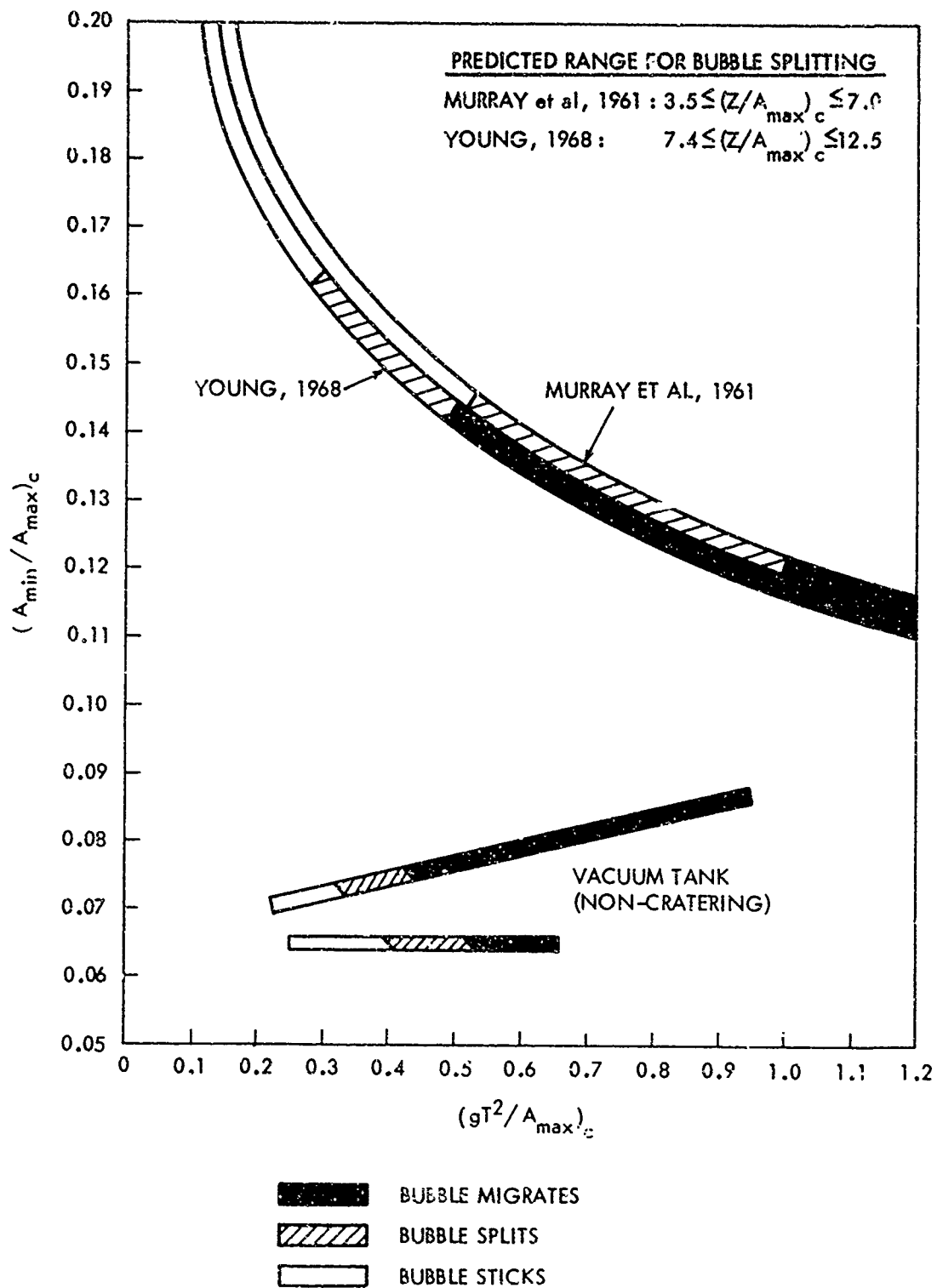


FIG. 17 COMPARISON OF NON-CRATERING MODEL BEHAVIOR
WITH ESTIMATES FROM FIELD TESTS

TABLE 1

EXPERIMENTAL DATA FROM SHOTS ON RIG. > BOTTOM

CHARGE: 0.2-gm dextronated lead azide lollypop

Shot Number	Water Temp. (°F)	Air Press. (ft of fresh water)	Charge Depth (ft)	(A _{max}) eg (ft)	D _{max} (ft)	H _{max} (ft)
IZ 0058 0059 PR 3090 3092 3093 3096 3097 3098 3117	80.5	5.72	1.00	.470	.924	.488
	80.0	5.72	1.06	.470	.979	.479
	71.7	4.75	2.00	.471	.935	.482
	71.6	3.58	2.00	.496	.982	.503
	71.5	3.88	2.00	.478	.940	.488
	71.5	3.96	2.00	.486	.958	.496
	71.5	4.33	2.00	.502	1.02	.525
	71.5	5.00	2.00	.451	1.08	.462
	84.5	5.72	1.04	.476	1.02	.486
	80.0	2.56	2.00	.488	.860	.511
IZ 0054 0055* PR 3091 3094 3109 3110 3118 3119 3120	80.5	2.58	2.00	.467	.795	.487
	71.8	2.85	2.00	.573	1.12	.592
	71.5	3.21	2.00	.500	.978	.490
	84.5	4.42	2.00	.475	1.09	.475
	84.5	4.10	2.00	.497	1.09	.504
	84.0	5.20	1.03	.486	1.00	.483
	84.0	4.70	1.03	.510	1.05	.510
	84.1	4.35	1.02	.519	1.07	.513

BUBBLE BEHAVIOR

Sticks

Splits

TABLE 1 (continued)

Shot Number	Water Temp. (°F)	Air Press. (ft of fresh water)	Charge Depth (ft)	(A _{max}) _{eq} (ft)	D _{max} (ft)	H _{max} (ft)
IZ 0056	80.5	2.05	1.00	.687	1.25	.718
0057	80.0	2.05	1.00	.686	1.29	.740
0060	79.5	3.47	1.00	.552	1.07	.581
0061	80.0	3.45	1.00	.559	1.06	.581
0062	80.0	2.56	1.00	.623	1.16	.645
0063	79.5	2.56	1.00	.622	1.19	.654
PR 3089	71.5	2.32	2.00	.548	1.04	.566
3095	71.5	2.00	2.00	.567	1.10	.596
3099	85.5	2.58	2.02	.563	1.10	.590
3100*	85.5	2.58	2.02	.621	1.17	.649
3101	85.5	2.58	2.02	.569	1.11	.606
3102	85.5	2.58	2.02	.569	1.11	.593
3103	85.5	2.58	2.02	.575	1.14	.580
3104	84.5	2.58	2.00	.601	1.16	.533
3105	85.5	2.58	2.00	.585	1.15	.602
3106	83.5	2.58	1.98	.614	1.20	.626
3107	84.5	2.58	1.98	.607	1.18	.613
3108	84.0	2.85	2.00	.589	1.08	.574
3111	85.7	3.55	2.00	.522	1.09	.520
3112	84.9	3.10	2.00	.561	1.09	.563
3113	84.5	2.40	2.00	.567	1.05	.563
3114	83.5	1.85	2.00	.656	1.26	.684
3115	84.5	2.20	2.00	.611	1.22	.623
3116	84.0	2.00	2.00	.617	1.22	.642
3121	84.5	4.07	1.00	.542	1.11	.543
3122	84.5	3.80	1.02	.558	1.15	.563
3123	84.5	3.60	1.00	--	1.14	.577
3124	84.5	3.45	1.00	.569	1.15	.565
3125	84.3	3.23	1.03	.578	1.15	.577
3126	84.5	3.00	1.03	.591	1.20	.596
3127	84.5	3.45	1.04	.563	1.14	.564
3128	83.7	3.45	1.00	.637	1.26	.651

BUBBLE MIGRATES INTACT

BUBBLE BEHAVIOR

* Measured data inconsistent--not included in the analysis of this report.

NOTE: IZ series of shots fired at Indian Head in 1952

TABLE 2

CHARACTERISTIC NUMBERS AND DIMENSIONLESS DATA FOR SHOTS ON RIGID BOTTOM

Shot Number	$\left(\frac{gT^2}{A_{\max}/c}\right)$	$\left(\frac{A_{\min}}{A_{\max}/c}\right)$	$\left(\frac{A_{\max}}{d}\right)^c$	$\frac{(A_{\max})^{eq}}{(A_{\max})^c}$	$\frac{D_{\max}}{(A_{\max})^c}$	$\frac{H_{\max}}{(A_{\max})^c}$	$\frac{H_{\max}}{D_{\max}}$
Sticks	YZ 0058	.243	.070	.406	1.15	2.27	.528
	0059	.242	.070	.381	1.16	2.42	.489
	PR 3090	.276	.064	.195	1.20	2.39	.515
	3092	.373	.064	.210	1.17	2.33	.572
	3093	.343	.054	.206	1.15	2.28	.519
	3096	.335	.064	.205	1.18	2.34	.517
	3097	.305	.064	.200	1.25	2.53	.519
	3098	.261	.065	.192	1.17	2.79	.430
	3117	.261	.074	.387	1.18	2.54	.474
Splitters	IZ 0054*	.552	.073	.240	1.01	1.78	.594
	0055*	.551	.073	.240	.97	1.65	.612
	PR 3091	.469	.064	.223	1.28	2.51	.528
	3094	.416	.064	.216	1.15	2.27	.496
	3109	.332	.074	.206	1.15	2.64	.437
	3110	.363	.075	.211	1.18	2.58	.463
	3118	.296	.074	.404	1.16	2.39	.482
	3119	.339	.075	.420	1.18	2.43	.482
	3120	.376	.076	.437	1.16	2.39	.481

TABLE 2 (continued)

Shot Number	$\left(\frac{gT^2}{A_{max} \sqrt{c}}\right)$	$\left(\frac{A_{min}}{A_{max} \sqrt{c}}\right)$	$\left(\frac{A_{max}}{d}\right)^{\frac{1}{c}}$	$\left(\frac{A_{max}^{eq}}{A_{max} \sqrt{c}}\right)$	$\frac{D_{max}}{\left(\frac{A_{max}}{A_{max} \sqrt{c}}\right)}$	$\frac{H_{max}}{\left(\frac{A_{max}}{A_{max} \sqrt{c}}\right)}$	$\frac{H_{max}}{D_{max}}$
0055	.935	.085	.591	1.16	2.10	1.21	.575
0057	.925	.084	.589	1.16	2.19	1.26	.573
0063	.463	.072	.484	1.13	2.21	1.20	.542
0063	.470	.073	.486	1.14	2.18	1.20	.548
0063	.693	.078	.542	1.14	2.14	1.19	.556
0063	.687	.077	.541	1.15	2.19	1.21	.549
PR 3063	.568	.064	.243	1.17	2.22	1.21	.544
3095	.647	.065	.242	1.16	2.25	1.23	.544
3099	.610	.080	.239	1.16	2.27	1.22	.536
3100*	.610	.080	.239	1.28	2.42	1.34	.554
3101	.610	.080	.239	1.17	2.29	1.25	.545
3102	.610	.080	.239	1.17	2.29	1.23	.534
3103	.610	.080	.239	1.19	2.36	1.20	.508
3104	.604	.079	.241	1.24	2.40	1.21	.502
3105	.613	.081	.242	1.20	2.37	1.24	.523
3106	.598	.078	.242	1.28	2.49	1.30	.521
3107	.607	.079	.244	1.25	2.44	1.31	.536
3108	.539	.077	.234	1.26	2.32	1.23	.529
3111	.433	.077	.221	1.18	2.45	1.18	.478
3112	.499	.077	.229	1.22	2.37	1.23	.516
3113	.651	.080	.246	1.15	2.14	1.15	.535
3114	.828	.082	.261	1.25	2.40	1.27	.526
3115	.712	.081	.251	1.21	2.42	1.24	.510
3116	.775	.082	.257	1.20	2.37	1.25	.526
3121	.414	.077	.449	1.18	2.41	1.18	.490
3122	.454	.078	.461	1.18	2.44	1.20	.489
3123	.489	.079	.480	--	2.37	1.20	.506
3124	.518	.080	.488	1.16	2.35	1.16	.491
3125	.564	.080	.484	1.15	2.30	1.16	.501
3126	.625	.083	.499	1.14	2.32	1.16	.498
3127	.517	.079	.468	1.15	2.34	1.16	.494
3128	.512	.078	.486	1.31	2.59	1.34	.516
Average				1.18	2.30	1.21	.513
s/Average (%)				3.6	5.9	4.0	6.0

* Measured data inconsistent--not included in standard deviation estimates or in the analysis presented in this report.

NOTES: (1) IZ series of shots fired at Indian Head in 1952.

(2) Standard deviation estimate, $s = \sqrt{\frac{\sum(x_i - \bar{x})^2}{n-1}}$

TABLE 3
MEASURED DATA AT FIRST BUBBLE MINIMUM FOR STRONGLY MIGRATING BUBBLES

Shot Number	$\left(\frac{gT^2}{A_{max}}\right) \frac{c}{c}$	$\left(\frac{A_{min}}{A_{max}}\right) \frac{c}{c}$	$\left(\frac{A_{max}}{d}\right) \frac{c}{c}$	τ (msec)	δ_{center} (ft)	δ_{top} (ft)	D_{min} (ft)	$\frac{\tau}{\tau_c}$	$\frac{\delta_{center}}{(A_{max})^c}$	$\frac{\delta_{top}}{(A_{max})^c}$	$\frac{D_{min}}{(A_{max})^c}$
1Z 0056	.935	.086	.591	142.1	.380	.550	.586	1.08	.642	.930	.991
FR 3089	.568	.064	.243	98.5	.295	.390	.310	1.08	.630	.833	.662
3099	.510	.080	.239	108.8	.334	.477	.458	1.14	.691	.987	.948
3100*	.510	.080	.239	119.2	.390	.556	.500	1.25	.808	1.150	1.035
3101	.610	.080	.239	109.5	.332	.466	.440	1.14	.687	.964	.910
3102	.510	.080	.239	108.4	.326	.451	.464	1.13	.674	.933	.960
3103	.610	.080	.239	109.5	.327	.452	.444	1.14	.678	.935	.919
3104	.604	.079	.241	111.5	.334	.464	.451	1.17	.693	.962	.935
3106	.598	.078	.242	114.3	.322	.446	.512	1.21	.670	.929	1.067
3095	.647	.065	.243	111.8	.329	.427	.340	1.13	.677	.880	.701
3112	.499	.077	.229	97.8	.281	.400	.383	1.16	.612	.873	.836
3113	.651	.080	.246	111.7	.320	.454	.464	1.12	.652	.924	.945
3114	.828	.082	.261	136.7	.413	.575	.549	1.18	.788	1.099	1.050
3115	.712	.081	.251	123.1	.368	.527	.517	1.17	.731	1.048	1.028
3116	.775	.082	.257	126.7	.375	.524	.507	1.14	.729	1.019	.986
Average											1.14
s/Average (%)											3.1

* Measured data inconsistent--not included in standard deviation estimate or in the analysis presented in this report.

APPENDIX A

CALCULATION OF MODEL PARAMETERS

The characteristic numbers $(gT^2/A_{\max})_c$, $(A_{\min}/A_{\max})_c$, and $(A_{\max}/d)_c$ for the model explosion were calculated using A_{\max} , T , and A_{\min} for the corresponding control shot (shot at identical test conditions in the Vacuum Tank except for the absence of the false bottom). These parameters, A_{\max} , T , and A_{\min}/A_{\max} (for the control), were calculated using the data and theory developed on previous test programs (Snay et al, 1952 and Goertner, 1956). Additional data from the present test program are listed in Tables A-1 and A-2. For this study, the experimental data for explosions in the Vacuum Tank (presented in previous reports as a collection of graphs) was recast as a set of empirical equations which enable computer computation of the model explosion parameters using test conditions as input.

The following paragraphs describe the empirical functions and theory for calculating A_{\max} , T , and A_{\min}/A_{\max} for the control. Further details can be obtained from the reports by Snay et al (1952) and Goertner (1956). In Appendix B, the major uncertainties in the present experimental data and theory will be discussed.

In the model explosion, two phenomena occur which do not occur in a prototype explosion. The first is a kinematic and dynamic interaction of the test tank with the explosion bubble. In the following discussion, the effects of tank interaction on the maximum bubble radius and bubble period are taken into account, but only approximately, by the empirical functions Ratio J^0 and Ratio K^0 (defined later-- read as "ratio J zero", etc.). The other phenomenon is evaporation or "boiling" of water into the bubble cavity when, near the bubble maximum, the pressure of the explosion gases falls below the vapor pressure of the surrounding water. This phenomenon is known as "boiling", and the empirical functions Ratio J^* and Ratio K^* (read as "ratio J star", etc.) are used to describe its effect on the maximum radius and bubble period, respectively.

EQUATIONS FOR A_{\max}

The maximum radius coefficient for the model explosion

$$J = A_{\max} \frac{Z^{1/3}}{W^{1/3}} \quad (A1)$$

where $Z = d + P_{\text{air}}$

= hydrostatic pressure at depth of explosion (ft of fresh water)

was determined experimentally as a function of test conditions in the vacuum tank. The radius coefficient was then represented as the product of three factors

$$J = J_{\infty} \times (\text{Ratio } J^0) \times (\text{Ratio } J^*) \quad (\text{A2})$$

These functions are defined below.

J_{∞} is the radius coefficient which would be measured in free water (no tank, no boiling) and at the same hydrostatic pressure. In this study, J_{∞} was taken to be a constant characteristic of the model explosive charge. (For the 1967 tests, $J_{\infty} = 9.09$; for the tests carried out in 1951 through 1953, $J_{\infty} = 9.21$.)

Ratio J^0 is the measure of the change, if any, in A_{\max} due to the presence of the test tank, i.e.,

$$\text{Ratio } J^0 = \frac{J \text{ in tank for non-boiling bubble}}{J_{\infty}} \quad (\text{A3})$$

at the same geometry with respect to the water surface. In this study, it is assumed that

$$\text{Ratio } J^0 = 1.0 \quad (\text{A4})$$

for the 0.2-gram model explosions.

Ratio J^* is the measure of the change in A_{\max} due to evaporation or "boiling" of water into the bubble, i.e.,

$$\text{Ratio } J^* = \frac{J \text{ in tank for boiling bubble}}{J \text{ in tank for non-boiling bubble}} \quad (\text{A5})$$

$$= \frac{J \text{ in tank for boiling bubble}}{J_{\infty} \times \text{Ratio } J^0} \quad (\text{A6})$$

$$= \frac{J \text{ in tank for boiling bubble}}{J_{\infty}} \quad (\text{A7})$$

since Ratio J^0 was assumed to be unity. Measurements of Ratio J^* are shown in Figure A-1. For this study, these measurements were represented by the equation

$$\text{Ratio } J^* = 1 + 0.64 \left[1 - \sqrt{1 - 1.45 \left(\frac{P_{\text{vap}}}{Z} \right)} \right] \quad (\text{A8})$$

where P_{vap} is the vapor pressure of the ambient water in feet of fresh water.

EQUATIONS FOR T.

The period coefficient, K:

$$K = T \frac{2^{5/6}}{W^{1/3}} \quad (A9)$$

was also determined experimentally as a function of the test conditions. The period coefficient was represented as the product of four factors

$$K = K_{\infty} \times \left(1 - \alpha \frac{A_{max}}{d}\right) \times (\text{Ratio } K^O) \times (\text{Ratio } K^*) \quad (A10)$$

These functions are defined as follows:

K_{∞} is the period coefficient which would be measured in free water remote from the surface and bottom and at the same hydrostatic pressure as the model explosion. In this study, K_{∞} was taken as a constant. (For the 1967 tests, $K_{\infty} = 3.21$; for the tests carried out in 1951 through 1953, $K_{\infty} = 3.20$.)

$\left(1 - \alpha \frac{A_{max}}{d}\right)$ is the correction factor for the water surface. No correction was made for the bottom. As in the earlier model studies (Snay et al, 1952 and Goertner, 1956) the value, $\alpha = 0.214$, was used for the surface correction coefficient*.

$\text{Ratio } K^O$ is the measure of the change in T due to the presence of the test tank, i.e.,

$$\text{Ratio } K^O = \frac{K \text{ in tank for non-boiling bubble}}{K \text{ in free water at same } A_{max}/d} \quad (A11)$$

$$= \frac{K \text{ in tank for non-boiling bubble}}{K_{\infty} \left(1 - \alpha \frac{A_{max}}{d}\right)} \quad (A12)$$

* This differs from the value $\alpha = 0.1$ previously used for the prototype explosion in Equation 5. In practice, values of α generally range from about 0.1 to about 0.3, apparently depending on the strength of the gravity migration. In the present modeling computations, this discrepancy is partially absorbed in the empirically determined "boiling" function, Ratio K^* . Ideally, the effect of gravity migration on K and J should be taken into account explicitly for both model and prototype calculations. However, as yet we are not able to do this.

It was assumed that Ratio K^0 was solely a function of the free-surface and tank-wall geometry for 0.2-gram explosions sufficiently far from the bottom for a non-yielding tank*. For this study, the existing data reported by Snay et al (1952, see Figure 24), was represented by the equation

$$\text{Ratio } K^0 = 1 + \frac{d}{R} \left[0.22 \frac{A_{\max}}{R} + 0.78 \left(\frac{A_{\max}}{R} \right)^2 \right] \quad (A13)$$

where R is the radius of the cylindrical tank**.

Ratio K^* is the measure of the change in T due to boiling, i.e.,

$$\text{Ratio } K^* = \frac{K \text{ in tank for boiling bubble}}{K \text{ in tank for non-boiling bubble}} \quad (A14)$$

$$= \frac{K \text{ in tank for boiling bubble}}{K_{\infty} (1 - \alpha A_{\max}/d) \text{ Ratio } K^0} \quad (A15)$$

where both bubbles have the same geometry with respect to the water surface and also with respect to the test tank. Measurements of Ratio K^* are shown in Figure A-2. These measurements were represented by the equation

$$\text{Ratio } K^* = 1 + 1.02 \left[1 - \sqrt{1 - 1.83 \left(\frac{P_{\text{vap}}}{Z} \right)} \right] \quad (A16)$$

EQUATIONS FOR A_{\min}/A_{\max}

For the non-boiling bubble, A_{\min}/A_{\max} was represented by

$$(A_{\min}/A_{\max})_o = N Z^{1/3} \quad (A17)$$

where the subscript "o" indicates the non-boiling case. The coefficient $N = 0.026$ for lead azide.

For model explosions in the vacuum tank, A_{\min}/A_{\max} is considerably greater than indicated by equation (A17) because of the boiling phenomenon. On the assumption that this evaporation takes place only at the lowest pressures, which occur relatively close to the bubble maximum, Snay et al (1952) developed an approximate theory for the increase in A_{\min}/A_{\max} due to boiling.

* Nevertheless, the distance of the charge from the bottom of the test tank was held approximately constant (= 50 inches), just in case.

** The simpler equation, $\text{Ratio } K^0 = 1 + 0.44 (d/R) (A_{\max}/R)$, also gives an adequate representation of this data.

The starting point for this calculation is the internal pressure at the time of the bubble maximum for a non-boiling bubble, $(P_{\max})_0$, which according to incompressible bubble theory (Snay and Christian, 1952) is given by:

$$\frac{(P_{\max})_0}{Z^{(\gamma-1)}} = \left(\frac{A_{\min}}{A_{\max}} \right)^{3(\gamma-1)} \frac{1 - (A_{\min}/A_{\max})_0^3}{1 - (A_{\min}/A_{\max})_0^{3(\gamma-1)}} \quad (A1B)$$

where $\gamma = 1.3$, the adiabatic exponent, for the lead azide explosion products (Snay et al, 1952).

Next, the pressure P_{\max} is calculated, which would occur at the time of the bubble maximum if the bubble motion after boiling has ceased could then be reversed (run backwards in time). This pressure is given by

$$\frac{P_{\max}}{(P_{\max})_0} = \left(\frac{\text{Ratio } K^*}{\text{Ratio } J^*} \right)^{3\gamma} \left(\frac{1 + 1.21 [(\text{Ratio } K^*)^3 - 1]}{1 + 1.12 [(\text{Ratio } K^*)^3 - 1]} \right) \quad (A19)$$

with again, $\gamma = 1.3$. ($\gamma = 1.3$ for water vapor, also.)

Finally, to obtain A_{\min}/A_{\max} , Equation (A1B) is used again, this time for the post-boiling bubble. Specifically, the equation

$$\frac{P_{\max}}{Z^{(\gamma-1)}} = \left(\frac{A_{\min}}{A_{\max}} \right)^{3(\gamma-1)} \frac{1 - (A_{\min}/A_{\max})^3}{1 - (A_{\min}/A_{\max})^{3(\gamma-1)}} \quad (A20)$$

was solved either graphically or by iteration for A_{\min}/A_{\max} .

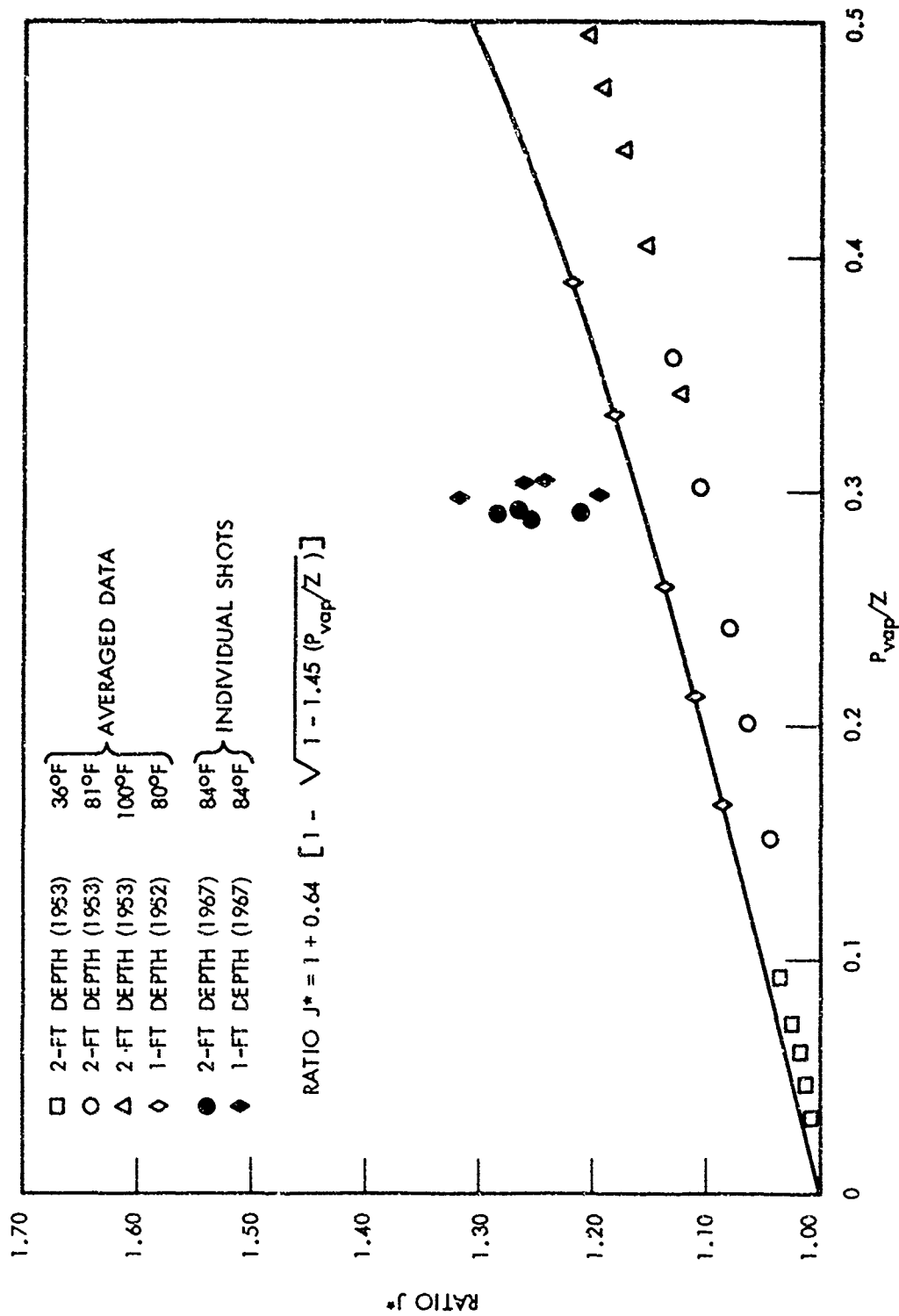


FIG. A-1 RATIO J^* AS A FUNCTION OF P_{vap}/Z FOR 0.2-gm LEAD AZIDE CHARGES IN NOL VACUUM TANK

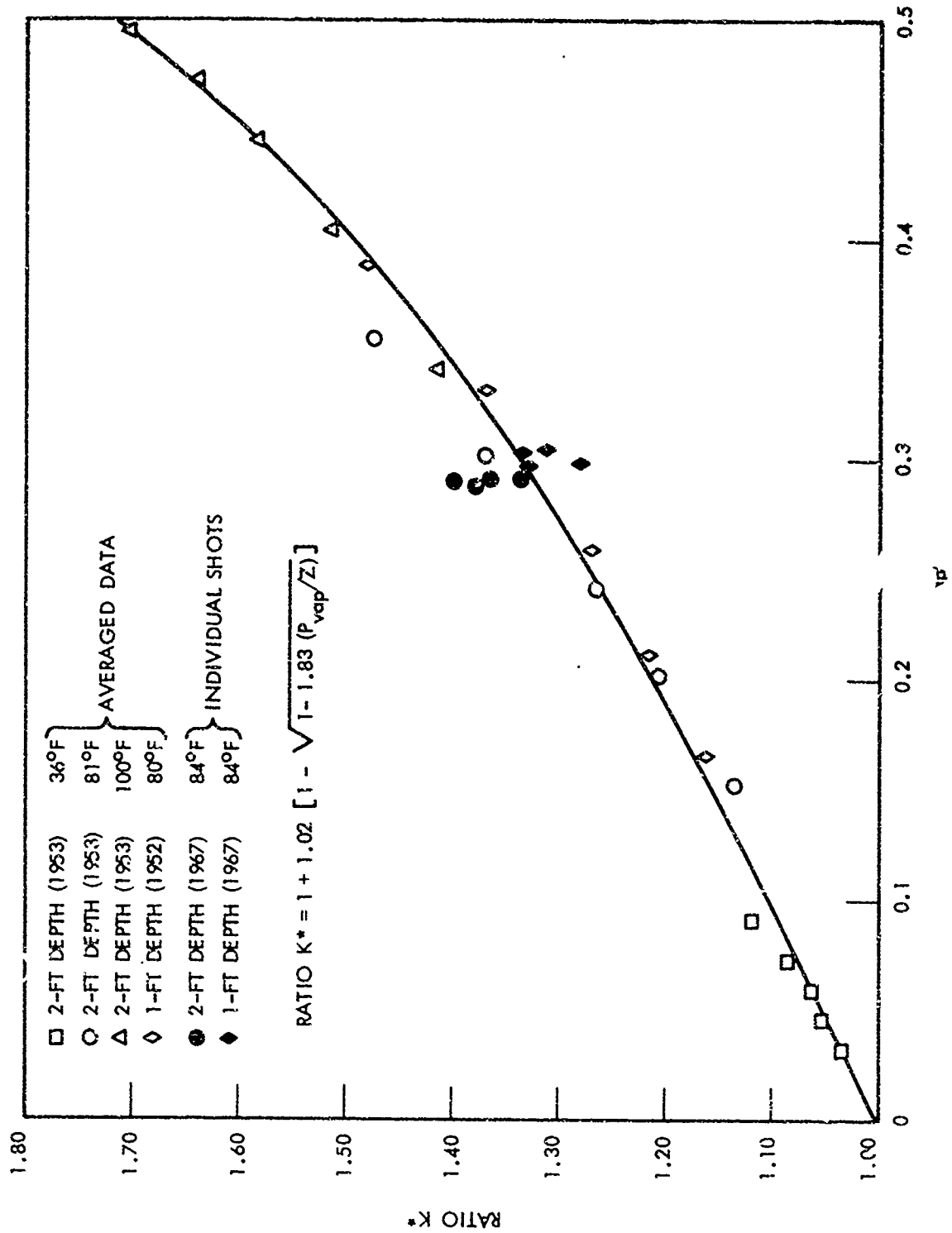


FIG. A-2 RATIO K^* AS A FUNCTION OF K^* FOR 0.2-gm LEAD AZIDE CHARGES IN NOL VACUUM TANK

TABLE A-1
EXPERIMENTAL DATA FROM CONTROL SHOTS--1967 TEST PROGRAM

CHARGE: 0.2-gm dextronated lead azide lollypop
Charge 4.2 feet from bottom of tank
AVERAGE WATER TEMPERATURE = 84.2°F

Shot Number	Air Pressure (ft fresh water)	Charge Depth (ft)	Water Temp. (°F)	T (msec)	$\frac{A_{max}}{(ft)}$	$\frac{\delta_{top}}{A_{max}}$	$\frac{\delta_{center}}{A_{max}}$
PR 3129	2.58	2.02	84.2	100.8	0.534	0.788	0.524
3130	2.58	2.01	84.1	98.3	0.527	0.805	0.535
3131	2.58	2.01	84.1	95.9	0.504	0.788	0.512
3132	2.58	2.02	84.0	99.1	0.521	0.779	0.516
Average s/Average (%)	2.58	2.02	84.1	98.5 2.0	0.521 2.4	0.790 1.3	0.522 1.9
PR 3133	3.45	1.05	84.1	87.4	0.552	0.497	0.262
3134	3.45	1.03	84.1	84.5	0.501	0.595	0.334
3135	3.45	1.01	84.7	86.5	0.522	0.539	0.309
3136	3.45	1.02	84.6	87.9	0.529	0.531	0.310
Average s/Average (%)	3.45	1.03	84.4	86.6 1.7	0.526 3.9	0.540 7.5	0.304 9.9

NOTE: Standard deviation estimate, $s = \sqrt{\frac{\sum (x_i - \bar{x})^2}{N-1}}$

TABLE A-2

COMPUTED DATA FROM CONTROL SHOTS--1967 TEST PROGRAM

Shot Number	K	J	Ratio K ^o	$\frac{P_{vap}}{Z}$	Ratio K*	Ratio J*	$\frac{gT^2}{A_{max}}$	$\frac{P_{max}}{Z}$	$\frac{A_{min}}{A_{max}}$	$\frac{A_{max}}{d}$
FR 3129	4.72	11.67	1.115	0.291	1.399	1.284	0.612	0.0278	0.065	0.264
3130	4.6	11.51	1.113	0.292	1.364	1.266	0.589	0.0265	0.062	0.262
3131	4.49	11.01	1.105	0.292	1.336	1.211	0.587	0.0290	0.068	0.251
3132	4.65	11.39	1.111	0.289	1.378	1.253	0.606	0.0238	0.067	0.258
Average	4.62	11.40	1.111	0.291	1.369	1.253	0.598		0.065	0.259
s/Average (%)	2.0	2.4	0.3		1.9	2.4	2.0		4.0	2.2
FR 3133	4.02	11.98	1.063	0.298	1.328	1.317	0.445	0.0203	0.047	0.526
3134	3.87	10.85	1.054	0.299	1.279	1.194	0.458	0.0255	0.059	0.486
3135	3.95	11.29	1.056	0.305	1.311	1.242	0.461	0.0241	0.056	0.517
3136	4.02	11.45	1.058	0.304	1.333	1.260	0.470	0.0245	0.057	0.519
Average	3.96	11.39	1.058	0.301	1.313	1.253	0.458		0.055	0.512
s/Average (%)	1.8	4.0	0.3		1.8	4.0	2.2		9.7	3.4

MOLIER 68-207

NOTES: (1) Ratio K^o was calculated from equation A13 using the measured value of A_{max} and R = 2ft.
 (2) The model test function, Ratio K--listed by Snay, et al, 1952, and Goertner, 1956--can be calculated from the equation, Ratio K = Ratio K^o x Ratio K*.

APPENDIX B

ANALYSIS OF UNCERTAINTIES IN THE MODEL TESTS

In Section 3.1, the equations for calculating the characteristic numbers for the prototype explosion were presented. In Appendix A, this was presented for the model explosion. Using both sets of equations, it is possible to calculate the model test conditions which correspond to a given prototype, or vice versa*.

In this appendix, estimates are given for the range of uncertainty in each model test parameter and how these uncertainties affect each of the three characteristic numbers for the model test. Similar treatment is then given for a typical HE field test. Finally, a discussion of the major sources of uncertainty in the model experiment and what can be done to improve the model experiment is discussed.

UNCERTAINTY ESTIMATES FOR MODEL AND PROTOTYPE TESTS.

Calculated model test conditions which correspond to a 100-pound TNT prototype at 30-foot depth are listed at the top of Table B-1. Next, estimates are listed for the range of uncertainty in each of the various inputs--experiment parameters, explosive parameters, empirical functions and boiling theory--needed to calculate the characteristic numbers for the model test. Using these estimates for the upper and lower limit of each input to the calculation, computations were made of the resultant change in each of the three characteristic numbers. These resultant uncertainties (partial differentials) are listed in the adjacent columns. Beneath each column, the square root of the sum of the squares of the partial differentials give a measure of the total experimental error (range) for each characteristic number.

Results of a similar analysis based on assumed uncertainties in the test and explosive parameters in a typical prototype test are listed below those for the model experiment.

Comparison of these error analyses for corresponding model and prototype tests shows that estimated uncertainties in the model results are significantly greater than those of the assumed prototype test. (This is even without examining the basic assumptions used to derive the modeling equations.) It will also be noted that this greater uncertainty estimate for the model results is caused by uncertainties as to

* Calculating the prototype test conditions which correspond to a given model experiment, however, is generally not very fruitful, because in practice, the prototype air pressure is generally restricted to one atmosphere; and only the size and depth of the explosion are at the experimenter's disposal. Model test conditions selected at random will generally result in prototype air pressures other than one atmosphere. Thus, only a small subset of realizable model conditions are in direct correspondence with realizable prototype conditions.

the accuracy of the boiling theory and the experimentally determined functions for boiling and tank interaction--Ratio K^* , Ratio J^* , Ratio K^0 , and Ratio J^0 .*

DISCUSSION OF UNCERTAINTIES IN THE BOILING AND TANK INTERACTION CORRECTIONS.

Boiling. The boiling theory (Snay et al, 1952) was developed to give a rough estimate of the increase in the explosion parameter A_{\min}/A_{\max} caused by boiling. There are no experimental data available for evaluating its accuracy; however, it is probably accurate to about ± 30 to 40%. As shown in Table B-1, this introduces a major uncertainty into the results from the vacuum tank tests. This uncertainty was one of the major reasons for constructing the NOL High Gravity Tank. However, as pointed out in Appendix C, the High Gravity Tank also has its problems.

At present, it appears to be technically feasible to make direct measurements of A_{\min} on the model scale by means of high-speed photographs at framing rates the order of 500,000 pictures per second. Preliminary efforts in this direction have been made using the NOL Vacuum Tank. However, in those tests it was not possible to accomplish meaningful measurements of A_{\min} because the bubble motion was distorted due to a dynamic interaction between the explosion and the test tank (discussed in next paragraph). When such tank interactions are better understood so that they can be controlled or taken into account, then photographic measurements of A_{\min} and its increase in the presence of boiling should provide a means toward improving the boiling correction.

Test Tank Interactions. Measurements of the explosion-induced motion of the front viewing window of the NOL Vacuum Tank were made by Sherman (1968). Comparison of those measurements with photographs of the bubble oscillation showed that the distorted bubble oscillation observed with non-migrating bubbles in the vacuum tank was due to flexing of the viewing windows. To date, this is the only direct observation of tank-bubble interaction in the vacuum tank. However, it appears that this is a general problem invalidating a basic assumption made in regard to the functions used to represent Ratio J^0 and Ratio K^0 , namely, that the test tank was rigid with respect to the bubble flow. Since Ratio J^0 and Ratio K^0 are used to calculate Ratio J^* and Ratio K^* (see Equations (A6) and (A15)), these two were affected. It seems probable that much of the scatter exhibited by the measured Ratio J^* and Ratio K^* data shown in Figures A-1 and A-2 was due to such unaccounted-for interactions with the test tank.

It is planned to test this hypothesis by installing stronger, more massive windows of smaller area which are designed to reduce the window motion (volume displacement) by about two orders of magnitude.

As a guide to the degree to which our knowledge of boiling and tank interaction effects should be improved, we have listed at the bottom of Table B-1 new uncertainty ranges for the boiling correction to A_{\min}/A_{\max} , Ratio K^* , Ratio J^* , Ratio K^0 , and Ratio J^0 which would make the total uncertainty in each of the characteristic numbers for the model experiment comparable to those for a prototype test. Total uncertainty ranges for the model characteristic numbers using these new inputs are listed at the bottom of the table.

* We have implicitly equated uncertainties in the characteristic numbers to uncertainties in model test results, since results from such model tests must be expressible as functions of the three characteristic numbers. A similar set of analyses was carried out for a 1000-pound TNT prototype explosion at 100-foot depth and yielded practically identical results (Goertner, 1968).

TABLE B-1
COMPARISON OF VACUUM TANK AND FIELD TEST UNCERTAINTIES
Corresponding model and prototype test conditions

Model Test		Characteristic Numbers		Prototype Test	
0.2 gas lead azide charge depth = 1.12 ft air pressure = 2.55 ft fresh water water temperature = 86.6°F		$gR^2/A_{max} = 0.812$ $A_{min}/A_{max} = 0.0915$ $A_{max}/d = 0.489$		100 lbs TNT charge depth = 30 ft air pressure = 33 ft sea water	
		Resulting Uncertainties (%)			
Input		Estimated Uncertainty	gR^2/A_{max}	A_{min}/A_{max}	A_{max}/d
PRESENT MODEL EXPERIMENT	Bubble energy, E	± 8%	± 2	0	± 3
	Water temperature, θ	± 2°F	± 4	± 6	± 1
	Charge depth, d	± 0.01 ft	0	0	± 1
	Air pressure, P _{air}	± 0.05 ft water	± 1	0	± 2
	Radius coefficient, J _u	± 3%	± 3	0	± 3
	Period coefficient, K _u	± 1%	± 2	0	0
	Free-surface coefficient, α	± 0.05	± 5	0	0
	$(A_{min}/A_{max})_0/Z^{1/3} = N$	± 10%	0	± 10	0
	Boiling theory ^{1/}	± 35%	0	± 35	0
	Ratio K*	± 5%	± 10	± 20	0
	Ratio J*	± 10	± 11	± 40	± 10
	Ratio K ^o	± 5%	± 10	0	0
	Ratio J ^o	± 10	± 11	0	± 10
		$\sqrt{\sum \Delta_1^2}$	± 17	± 58	± 15
FIELD TEST	Bubble energy, E	± 15%	± 4	0	± 5
	Charge depth, d	± 1 ft	± 2	± 1	± 4
	Air pressure, P _{air}	± 5%	± 3	± 1	± 1
	Radius coefficient, J _u	± 5%	± 6	0	± 5
	Period coefficient, K _u	± 3%	± 6	0	0
	Free-surface coefficient, α	0.05	± 5	0	0
	$(A_{min}/A_{max})_0/Z^{1/3} = N$	± 10%	0	± 10	0
		$\sqrt{\sum \Delta_1^2}$	± 11	± 10	± 8
A revised estimate for the model experiment assuming improved knowledge of the effects of tank interaction and boiling.					
FUTURE MODEL EXPERIMENT ²	Boiling theory	± 10%	0	± 10	0
	Ratio K*	± 3%	± 6	± 12	0
	Ratio J*	± 3%	± 3	± 12	± 3
	Ratio K ^o	± 2%	± 4	0	0
	Ratio J ^o	± 2%	± 3	0	± 2
		$\sqrt{\sum \Delta_1^2}$	± 11	± 17	± 6

^{1/} This variation was inputted to the computation by multiplying the calculated A_{min}/A_{max} for the model explosion by either 1.35 or 0.65.

APPENDIX C

HIGH-GRAVITY TANK TESTS ON A BOX-CRATERING BOTTOM

As mentioned in the introduction, one purpose of the 1967 series was to resolve an apparent discrepancy between the bubble behavior observed in the NOL Vacuum Tank during the 1952 program of bottom-shot tests and a series of model tests carried out in the High-Gravity Tank by Sherman (1965). The original High-Gravity Tank installation using the Sandia Corporation's centrifuge was described in detail by Price, Zuke, and Infosino (1964). Some of the later modifications incorporated into the present installation at NOL were briefly described by Bartlett (1969).

The bubble migration behavior from the G-tank test series is shown in Figure C-1 as a function of the characteristic numbers $(gT^2/A_{\max})_c$ and $(A_{\min}/A_{\max})_c$ for control shots at the same test conditions. No instances of bubble sticking were observed. On the deepest shot-- $(gT^2/A_{\max})_c = 0.25$ --the bubble split into two parts, both of which migrated upward. The upper portion accounted for some 70% of the total volume.

On these tests, the transition from splitting to migrating was very gradual and occurred somewhere within the range $0.4 \leq (gT^2/A_{\max})_c \leq 1.0$. These borderline observations are indicated by the symbol "?" in Figure C-1.

Depth-versus-time trajectories for the top of either the bubble or the upper portion of the splitting bubble were measured and compared with those from corresponding control shots. Significant difference between these trajectories (retardation of the bottom-shot bubble) was observed only for the two deepest conditions. This indicated that possibly the questionable cases should be classified as migrating bubbles, which would put the transition from splitting to migrating at about $(gT^2/A_{\max})_c = 0.5$.

On neither of the two conditions where the bubble was observed to split did the lower portion remain pulsating on the bottom.

The migration behavior just described is quite different from that observed in the Vacuum Tank where the entire transition, sticking to migrating, took place as $(gT^2/A_{\max})_c$ increased by 0.1 units. It is also quite different from that inferred from full scale tests over cratering bottoms, where instances of the bubble sticking to the bottom appear to have occurred.

The very gradual transition from splitting to migrating may be due to the fact that the High-Gravity Tank bubbles, like full-scale bubbles, pulsate more weakly than those in the Vacuum Tank. The fact that there were no sticking bubbles observed in the High-Gravity Tank tests may be due to the different effects of cratering and non-cratering bottoms. However, there is limited evidence of a strong interaction between the test tank and the explosion at the conditions employed for these experiments, and it has not been possible to verify that the oscillation and migration of control shots in the High-Gravity Tank is in agreement with full-scale bubble behavior. No firm interpretation of these tank data is possible until this question is resolved.

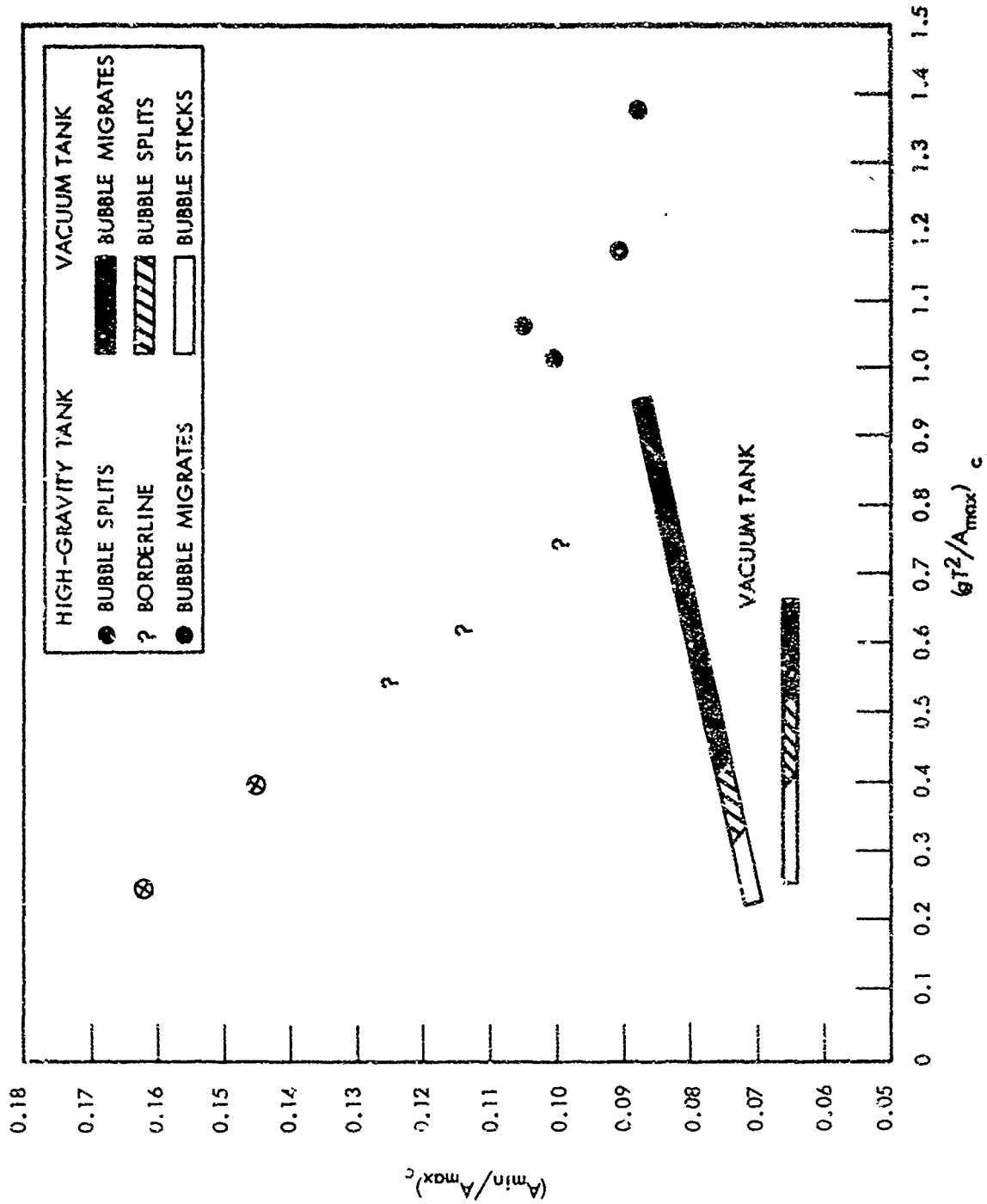


FIG. C-1 BEHAVIOR OF HIGH-GRAVITY TANK BUBBLES ON A NON-CRATERING BOTTOM AS A FUNCTION OF $(gT^2/A_{max})^c$ AND $(A_{min}/A_{max})^c$

APPENDIX D

EXPERIMENTAL DETAILS

The experiments were carried out with small charges in the NOL Vacuum Tank (see reports by Smay, Goertner, and Price, 1952; Goertner, 1956; and Zuke, 1960). This static tank is an upright steel cylinder with a removable lid. It is 4 feet in diameter and 11 feet 4 inches high on the inside. Its lower section (7 feet 2 inches high) has a 1-inch thick wall and two opposing 18 x 36 x 1-inch tempered plate glass viewing windows (Figures 1 and 2; Smay, Goertner, and Price, 1952).

For the present tests, the lower section was partially filled with tap water which was then filtered with a diatomaceous earth filter attached to the tank. Reduced air pressure above the water was obtained with a five HP Stokes Microvac pump. This pump was also used in conjunction with a mechanical pounder (Figure 1-c, Goertner, 1956) to de-aerate the water prior to starting the tests and at four to five shot intervals thereafter. De-aeration time was about one hour using an air pressure near the vapor pressure of the water.

The water temperature was controlled by circulating through either a 6KW heater or a 3HP chiller. Measured water temperatures are believed accurate to within $\pm 2^\circ$ F. The air pressure over the shot was measured with a Wallace and Tiernan Model FA 173 closed mercury manometer. Measured air pressures are believed accurate to within ± 0.05 feet of water.

To simulate the effect of a rigid non-yielding bottom, a false bottom consisting of a 2-inch thick by 44-inch diameter aluminum plate bolted to a heavy steel stand was placed in the tank. Beyond the maximum radius expected for the bubble, two metal pins protruded from the bottom to provide a linear scale for the photographs.

The charge* was of the so-called "lollipop design" (Zuke, 1961) constructed from two 0.2-inch diameter hemispheres of unmilled dextrinated lead azide cemented together around a sliver of printed circuit board. The assembled charge was water-proofed with a dip-coating of Magic Vulc latex compound. The charge was initiated by exploding the 0.031-inch long by 0.001-inch diameter Tophet C bridgewire with a 2300V-4 μ F discharge. The shot-to-shot standard deviation of the period and radius coefficients for these charges is estimated from previous work to be about $\pm 2\%$.

For the bottom shots, the charge was located with the stem horizontal with its center 0.2 inch (two charge radii) from the aluminum plate** It was estimated that this was close enough to the plate to simulate a bottom shot yet far enough away that the plate would not yield or crater. In order to check this assumption, one firing condition was repeated nine times--three times with each of the following standoffs: 1, 2, and 5 charge radii. No significant differences in bubble behavior were detected for these three standoffs.

Motion pictures (3000 frames/second) were taken of each shot using a 16mm Eastman High Speed camera. One-millisecond timing marks were placed on one edge of the film. Silhouette lighting was provided by a 375-watt photoflood bulb overvolted.

* Manufactured for NOL by Maryland Assemblies Inc., Port Deposit, Maryland.

** Charge located at center of tank 50 inches from bottom.

HOLAR 68-207

at 135 volts and imaged on the camera lens with a 25 x 20-inch Fresnel lens placed behind the rear window. The photographs were taken with Kodak Linagraph Shellburst film developed 20 minutes in D-19 at 68°F*.

* In interpreting and measuring photographs of underwater explosion bubbles, additional recorded detail is needed in the photographs in order to distinguish the outline of the explosion bubble from clouds of small air bubbles and other debris suspended in the water. For this purpose, it appears that color film or medium contrast black and white film would have been better.

DISTRIBUTION LIST

	Copies
Chief of Naval Operations Washington, D. C. 20360 Attn: OP-75	1
Chief of Naval Research Washington, D. C. 20360 Attn: Code 408 Code 418 Code 466 Code 468	1 1 1 1
Commander Naval Ordnance Systems Command Washington, D. C. 20360 Attn: ORD-033 ORD-0341 ORD-035 ORD-054111 ORD-05411 ORD-9132	1 1 1 2 1 2
Commander Naval Ships Systems Command Washington, D. C. 20360 Attn: NADSC-6423 Code 0352	2 1
Commander Naval Facilities Engineering Command Washington, D. C. 20360	1
Commanding Officer Naval Radiological Defense Laboratory San Francisco, California 94135 Attn: Code 222 Code 911 Code 934 Code 908D2	1 1 1 2
Commanding Officer U. S. Naval Ordnance Station Indian Head, Maryland 20640 Attn: Library Division	1
Commanding Officer U. S. Naval Explosive Ordnance Disposal Facility Indian Head, Maryland 20640 Attn: Library Division	1

DISTRIBUTION LIST (continued)

	Copies
Commander Naval Weapons Laboratory Dahlgren, Virginia 22448 Attn: Experimental Officer	1
Commander Naval Weapons Center China Lake, California 93555 Attn: Technical Library	1
Commander Naval Undersea Warfare Center 3202 E. Foothill Boulevard Pasadena, California 91107	1
Director Naval Research Laboratory Washington, D. C. 20390	2
Commanding Officer & Director Naval Ship Research & Development Center Washington, D. C. 20007 Attn: Library	1
Dr. W. W. Murray	1
Commanding Officer & Director Underwater Explosions Research Division Naval Ship Research & Development Center Portsmouth, Virginia 23709	1
Superintendent U. S. Naval Postgraduate School Monterey, California 93940	1
Commander Naval Undersea Warfare Center San Diego Division 271 Catalina Boulevard San Diego, California 92152	1
Commanding Officer U. S. Naval Underwater Weapons Research & Engineering Station Newport, Rhode Island 02840	1
Commander U. S. Naval Weapons Station Yorktown, Virginia 23491 Attn: Research & Development Division	1

DISTRIBUTION LIST (continued)

	Copies
Commanding Officer Naval Torpedo Station Keyport, Washington 98345	1
Commanding Officer U. S. Navy Underwater Sound Laboratory Fort Trumbull New London, Connecticut 06320	1
Commanding Officer U. S. Naval Air Development Center Johnsville, Pennsylvania 18974	1
Commander U. S. Naval Oceanographic Office Washington, D. C. 20390	1
Commanding Officer U. S. Navy Mine Defense Laboratory Panama City, Florida 32402	1
Commanding Officer Naval Civil Engineering Laboratory Port Hueneme, California 93041	1
Commanding Officer U. S. Naval Weapons Evaluation Facility Kirtland Air Force Base Albuquerque, New Mexico 87117	1
Chief of Research & Development Department of the Army Washington, D. C. 20310	2
Commanding General Material Command Headquarters Department of the Army Washington, D. C. 20315	2
Chief of Engineers Department of the Army Washington, D. C. 20315 Attn: ENGNB ENGEB	2 1
Commanding Officer U. S. Army Mobility Equipment R&D Center Fort Belvoir, Virginia 21060	2

DISTRIBUTION LIST (continued)

	Copies
Director	
Waterways Experiment Station	
Vicksburg, Mississippi 39181	1
Attn: Technical Library	1
G. L. Arbuthnot	1
J. N. Strange	
Commanding General	
Ballistic Research Laboratories	
Aberdeen, Maryland 21005	1
Commanding Officer	
Picatinny Arsenal	
Dover, New Jersey 07801	1
Commanding Officer	
USA Signal R&D Laboratory	
Fort Monmouth, New Jersey 07703	1
Attn: Technical Documents Center	
Commanding Officer	
Nuclear Defense Laboratory	
Edgewood, Maryland 21010	1
Chief	
AF Technical Applications Center	
2525 Telegraph Road	
Alexandria, Virginia 22300	1
Commander (OQAMA)	
Hill Air Force Base	
Ogden, Utah 84401	1
Attn: Ammunition Services Office	
Commander (PGTRI)	
Air Proving Ground Center	
Eglin Air Force Base, Florida 32542	1
Commander	
Norton Air Force Base	
San Bernadino, California 92409	1
Attn: SMASB	
Commander	
Air Force Weapons Laboratory	
Kirtland Air Force Base	
Albuquerque, New Mexico 87117	1
Attn: WILL	

DISTRIBUTION LIST (continued)

	Copies
Director Defense Research & Engineering Washington, D. C. 20310 Attn: Technical Library	1
Director Applied Physics Laboratory Johns Hopkins University Silver Spring, Maryland 20910	1
Director Defense Atomic Support Agency Washington, D. C. 20305 (SPLN)	2 1
Director Applied Physics Laboratory University of Washington Seattle, Washington 98105	1
Director Ordnance Research Laboratory Pennsylvania State University University Park, Pennsylvania 16802	1
Director Woods Hole Oceanographic Institution Woods Hole, Massachusetts 02543	1
Director Scripps Institute of Oceanography La Jolla, California 92037	1
Director Lawrence Radiation Laboratory University of California Livermore, California 94024 Attn: Technical Information Division	2
Director Los Alamos Scientific Laboratory University of California P. O. Box 1663 Los Alamos, New Mexico 87544 Attn: Dr. D. P. MacDougall	2
NASA Scientific & Technical Information Facility P. O. Box 33 College Park, Maryland 20740	1

DISTRIBUTION LIST (continued)

Copies

Sandia Corporation Sandia Base Albuquerque, New Mexico 87115 Attn: Information Distribution Section	1
Sandia Corporation P. O. Box 969 Livermore, California 94551	1
URS Corporation 1811 Trousdale Drive Burlingame, California 94011 Attn: Kenneth Kaplan Deputy Director	1
Chief of Naval Material U. S. Naval Ordnance Laboratory White Oak, Silver Spring, Maryland 20910 Attn: ASW-900 (A. Solem)	1
Commanding Officer Naval Weapons Center Corona Laboratories Corona, California 91720	1
Commanding Officer U. S. Army Combat Development Command Nuclear Group Fort Bliss, Texas 79906 Attn: Effects Division	1
Commanding Officer U. S. Army Corps of Engineers Coastal Engineering Research Center Washington, D. C. 20315	1
Chief Classified Technical Library Technical Information Service U. S. Atomic Energy Commission Washington, D. C. 20545	1
VESIAC Institute of Science and Technology University of Michigan Box 618 Ann Arbor, Michigan 48107	1

DISTRIBUTION LIST (continued)

	Copies
Air Force Technical Applications Center Hq. U. S. Air Force Washington, D. C. 20333 Attn: VELA Seis. Center	1
Air Force Cambridge Research Laboratories L. G. Hanscom Field Bedford, Massachusetts 01731 Attn: CRJW	1
Air Force Office of Scientific Research Washington, D. C. 20333 Attn: Geophysics Division	1
Institute for Defense Analyses 400 Army-Navy Drive Arlington, Virginia 22202 Attn: Mr. Rubenstein	1
Underwater Systems, Incorporated World Building, Room B-10 8121 Georgia Avenue Silver Spring, Maryland 20910 Attn: Dr. Marvin S. Weinstein	1
U. S. Atomic Energy Commission Division of Military Application Washington, D. C. 20545	3
Isotopes, Inc. 4062 Fabian Street Palo Alto, California 94303 Attn: Dr. Schink	1
Tetra-Tech, Inc. 630 N. Rosemead Boulevard Pasadena, California 91107	1
U. S. Arms Control and Disarmament Agency Department of State Washington, D. C. 20452 Attn: Dr. Basore Science & Tech. Division Colonel Dr. H	1 1 1 1
Nuclear Test Detection Advanced Research Projects Agency Room 3D170, The Pentagon Washington, D. C. 20301	3

DISTRIBUTION LIST (continued)

	Copies
Headquarters USAF (Air Force Technical Applications Center) 6801 Telegraph Road Alexandria, Virginia 20333 Attn: Dr. G. Leies Mr. Walter Singlevich	1 1
Mr. Arthur Barber Deputy Asst. Secretary of Defense International Security Affairs (Arms & Trade Control) The Pentagon Washington, D. C. 20301	1
Joint Chiefs of Staff Office of Special Assistant for Arms Control Department of Defense, the Pentagon Washington, D. C. 20301	1
McClellan Central Laboratory 1155th Technical Operations Squadron, USAF McClellan Air Force Base California 95652 Attn: Major Jackie T. Phelps Chief, Support Section	1
Defense Documentation Center Cameron Station Alexandria, Virginia 22314 Attn: TISIA-2	20
Chief of Naval Material Washington, D. C. 20360 Attn: NMAT-03 DPL-NMAT-03L NMAT-0312D	1 1 1

UNCLASSIFIED

Security Classification

DOCUMENT CONTROL DATA - R & D

(Security classification of title, body of abstract and indexing annotation must be entered when the overall report is classified)

1. ORIGINATING ACTIVITY (Corporate author)		2a. REPORT SECURITY CLASSIFICATION	
U. S. Naval Ordnance Laboratory White Oak, Silver Spring, Maryland 20910		Unclassified	
3. REPORT TITLE		2b. GROUP	
MODEL STUDIES OF THE BEHAVIOR OF UNDERWATER EXPLOSION BUBBLES IN CONTACT WITH A RIGID BOTTOM			
4. DESCRIPTIVE NOTES (Type of report and inclusive dates)			
Interim			
5. AUTHOR(S) (First name, middle initial, last name)			
John F. Goertner John R. Hendrickson Richard G. Leamon			
6. REPORT DATE	7a. TOTAL NO. OF PAGES	7b. NO. OF REFS	
6 March 1969	v1 +58	18	
8a. CONTRACT OR GRANT NO.	9a. ORIGINATOR'S REPORT NUMBER(S)		
NRDL Work Request 7-0069	NOLTR 68-207		
b. PROJECT NO.	9b. OTHER REPORT NO(S) (Any other numbers that may be assigned this report)		
Task No. NOL-150/NRDL			
c.			
d.			
10. DISTRIBUTION STATEMENT			
This document may be further distributed by any holder <u>only</u> with specific prior approval of NOL.			
11. SUPPLEMENTARY NOTES		12. SPONSORING MILITARY ACTIVITY	
		Advanced Research Projects Agency Washington, D. C. 20301	
13. ABSTRACT			
<p>The behavior of the explosion bubble in contact with a rigid bottom was investigated on a small scale using high speed photography. The experiments were carried out in a vacuum tank with 0.2-gram charges fired above a 2-inch thick aluminum plate. Test conditions were varied by small increments so that a complex sequence of changing bubble behavior--from bubbles which remained intact on the bottom, to bubbles which split into two or more parts, to bubbles which separated from the bottom intact--was observed. A qualitative description of the bubble behavior along with its dimensions at maximum volume and--for strongly migrating bubbles--at minimum volume is presented in dimensionless form as a function of the inverse Froude number, the amplitude of oscillation, and the distance to the water surface. The qualitative behavior appears to be different from that observed with HE field tests on cratering bottoms. Other factors being equal, there appears to be a greater tendency for a bubble to stick to a cratering bottom.</p>			

DD FORM 1473 (PAGE 1)

S/N 0101-807-6801

UNCLASSIFIED

Security Classification

